Journal of Structural Geology, Vol. 13, No. 5, pp. 557 to 578, 1991
Printed in Great Britain

0191-8141/91 $03.00+0.00

Structural analysis of progressive deformation within complex transcurrent shear zone systems: southern Narragansett Basin, Rhode Island

SHARON MOSHER and ALAN W. BERRYHILL

Department of Geological Sciences, University of Texas at Austin, Austin, TX 78713, U.S.A.

(*Received* 28 *October* 1989; *accepted in revised form* 11 *December* 1990)

Abstract—Complex progressive ductile deformation on Dutch Island, Narragansett Basin, Rhode Island, is localized along a system of non-parallel, intersecting shear zones with opposite senses of strike- and oblique-slip motion. The structural intensity and complexity of this area can be attributed in part to the proximity of NNE-, NE- and ENE-trending, pre-existing basement faults bounding early horsts and grabens. Reactivation of these faults caused the formation of shear zones within the overlying metasediments. Structural superposition of non-coaxial mesoscopic folds and crenulation cleavages, formed as a result of progressive movement along these shear zones, provide unusual and accurate kinematic indicators that track movement along individual zones through time. Sinistral motion on NNE-trending zones preceded dextral motion on NE-trending zones. Dextral oblique-slip motion on ENE-trending zones followed. Deformation became increasingly brittle with time. The deformation is the result of two transcurrent shear systems with opposite senses of motion that formed adjacent to the North American and African plate boundary after plate collision.

INTRODUCTION

THE Narragansett Basin of Rhode Island and Massachusetts (Fig. 1) is a critical area for understanding the Alleghanian orogeny in the northern Appalachians. The Pennsylvanian-age basin is an elongate structural basin believed to be part of a NE-trending chain of grabens extending offshore to the NE and SW under Long Island Sound (McMasters *et al.* 1980, Mosher 1983). Following initial rifting and subsequent filling of the basin, convergence of Africa and North America closed the basin in early Permian time (Mosher 1983), producing a sequence of basin-wide deformations concentrated in the southern part of the basin. The sequence of post-rifting deformation may be subdivided into four major deformational events (Mosher 1983): D_1 and D_2 may be attributed to initial basin closure, producing large-scale, overturned to recumbent, isoclinal to open folds with opposite senses of vergence and pronounced axial planar cleavages. Concurrent with these early folding events was a high-grade regional metamorphism which reached kyanite–sillimanite grade at the western margin of the basin (Grew & Day 1972, Skehan & Murray 1979). D_3 and D_4 were caused by movement along large-scale, non-parallel sinistral and dextral transcurrent shear zones, respectively, which apparently overlie reactivated faults bounding intrabasinal horsts and grabens (Henderson & Mosher 1983, Mosher 1983). These deformations produced a large and complex variety of structures, including folds, crenulation cleavages, boudins, sheath folds, tension gashes, kink bands and faults, which are expressed to varying degrees throughout the basin. Finally, a period of brittle deformation produced two sets of conjugate joints and minor normal and block faulting.

The detailed structural study reported here was conducted adjacent to one of the complex D_3–D_4 shear systems, to determine the deformational sequence within the shear system and to relate the structures and their relative times of occurrence to the tectonic framework for the Narragansett Basin in the Late Paleozoic. This study examines Dutch Island, located in southwestern Narragansett Basin, within the Beaverhead shear zone (Fig. 1). The island is a fault-bounded horst block, eroded to its present state by Pleistocene glaciation. The rocks on Dutch Island preserve a deformational sequence as intense and complex as is found anywhere in the basin. Two distinct generations of shear zones with opposite senses of strike-slip motion generated two major progressive deformations, overprinting a preexisting metamorphic and structural fabric. This study combines a geometric analysis of microscopic and mesoscopic structures found on Dutch Island with a comparative study of incremental strains produced during progressive deformation within a shear zone to determine the precise movement history of transcurrent shear zones in the southern Narragansett Basin.

Previous work

Prior to this study, only reconnaissance lithologic and structural mapping had been conducted on Dutch Island. Shaler *et al.* (1899) listed and described the basic lithologies on Dutch Island and assigned a Pennsylvanian age to the metasediments on the basis of plant fossil identification. Preliminary structural mapping by Burks (1981) and Murray (unpublished data) indicated a highly complex structural history, possibly similar to the deformational sequence found on nearby Beaverhead (Skehan & Murray 1979, Burks 1981). Skehan & Murray

(1979) attributed areas of intense deformation in the southern basin to proximity to major strike-slip faults, and Mosher (1983) proposed a kinematic model for the Narragansett Basin that allows for the structural intensity and complexity found on Dutch Island.

Field techniques

Dutch Island has continuous outcrop along three-quarters of the coastline, allowing detailed structural mapping at a scale varying from 1:60 to 1:1200, depending on outcrop quality and structural complexity. The most continuous outcrop was found in the southern portion of the island. The majority of the interior of the island is covered by glacial till and dense vegetation. The scale of mapping conducted on Dutch Island allowed discrimination of small-scale structures that might have been lumped together in a more regional study. In addition, joint surfaces provide three-dimensional exposures around much of the island, so that precise measurements of fold axes and cleavage planes were possible. This three-dimensional geometric analysis aided considerably in differentiating similar structures produced during progressive deformation.

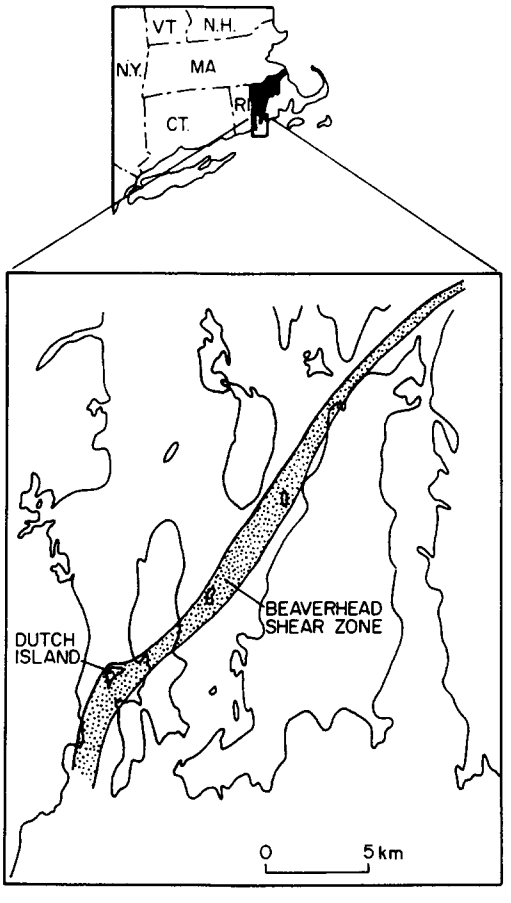

Fig. 1. Location map for Narragansett Basin (shown in black), Dutch Island, and Beaverhead shear zone. The NE-trending Beaverhead shear zone contains the most intensely deformed rocks in the basin and consists of a series of short, interconnected, NNE-, NE- and ENE-trending shear zone and fault segments.

Lithology

The rocks exposed on Dutch Island lie within the Pennsylvanian Rhode Island Formation (Mutch 1968). All rocks on Dutch Island exhibit metamorphic mineral assemblages within the almandine zone and have undergone varying degrees of retrograde metamorphism and chloritization. The major lithology on Dutch Island is a gray to black phyllite; minor lithologies include brown to green psammite, metaconglomerate, carbonaceous black phyllite and, locally, calcsilicate pods.

STRUCTURE

Introduction

The deformational history of Dutch Island, after the formation of the Narragansett Basin, may be subdivided into four major events. The first two events produced two to three generations of discrete folds and associated structures. The third and fourth deformations were caused by sinistral and dextral strike-slip motion on NNE-, NE- and ENE-trending shear zones, respectively. These deformations fit within the tectonic framework proposed for the Narragansett Basin by Mosher (1983) and similar deformational sequences were described elsewhere in the basin in field studies by Burks (1981, 1985), Thomas (1981), Farrens (1982), Henderson & Mosher (1983), Reck (1985) and Reck & Mosher (1989). Thus, the sequence and style of deformation found on Dutch Island is not unique within the basin; however, the intensity and complexity of structures has not been previously recognized elsewhere in the basin. The extraordinary quality of preservation of deformational features allows a detailed geometric and kinematic analysis of structures produced by progressive noncoaxial deformation.

An overview of structural styles on Dutch Island shows that deformational complexity and intensity are not uniform across the island. On both sides of the island the structural style changes significantly across a fairly abrupt boundary (marked SSC on Fig. 2 and all subsequent maps). South of this boundary, shear-related deformation is more complex and widespread, and early D_1 and D_2 structures are almost completely transposed. The structure of Dutch Island will be described in two parts: early deformation and metamorphism, and all deformation related to later strike-slip movement.

Early deformation and metamorphism

Post-rifting deformation on Dutch Island began with polyphase folding. Two distinct open to isoclinal folding events (F_1 and F_2) with associated axial planar, subparallel foliations (S_1 and S_2) are present on Dutch Island (Fig. 2). Concurrent metamorphism reached garnet grade. The significant result of early deformation and metamorphism on Dutch Island was the formation of a pervasive structural and metamorphic fabric which

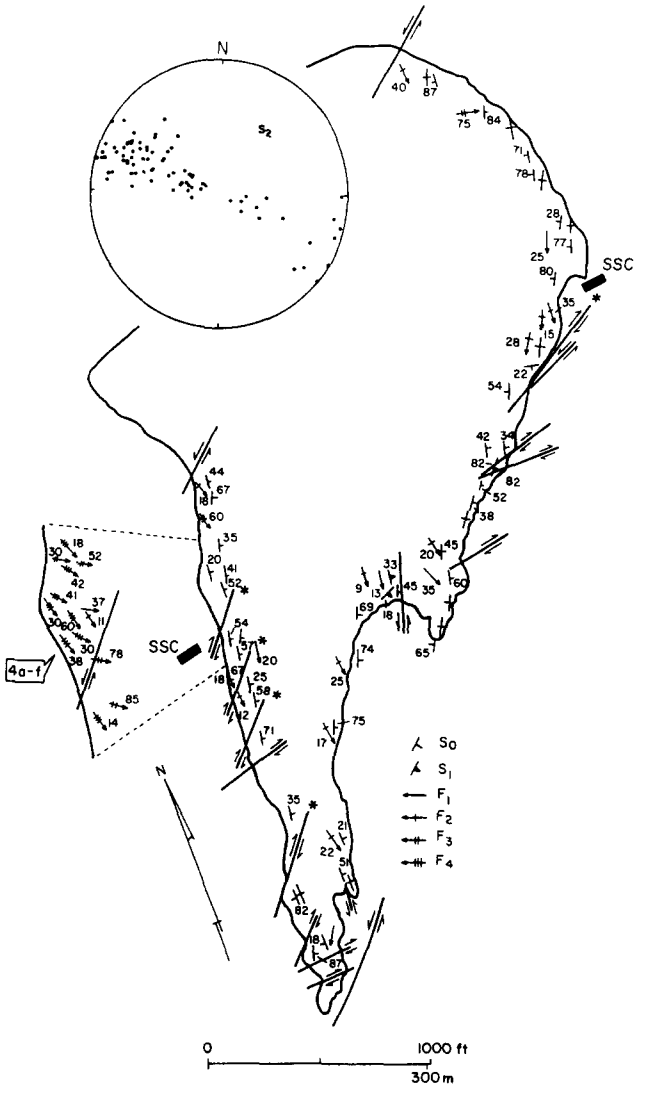

Fig. 2. Structural map of S_0, S_1, F_1, F_2, F_3 and F_4 on Dutch Island and stereoplot of S_2 poles. (All stereoplots are equal-area, lower-hemisphere projections.) S_2 is not included on the map because of its extremely variable and pervasive character. Blow-up of NW coastline shows orientation of folds in discrete sinistral shear zones. Note that all but one of the F_3 and F_4 folds are found in this area; the exception is found in a discrete sinistral shear zone on the NE coastline. S_1 is only measurable at one location in the field; in the hinge of a large F_1 fold. SSC (on all maps) stands for structural style change boundary (see text for discussion). Only major shear zones are shown (on all maps except Fig. 3); zones with two directions of motion are indicated by *, and only the second direction of motion (dextral) is indicated. Locations of Fig. 4(a)–(f) shown.

allowed excellent preservation of later deformation features.

Outcrop examples of F_1 and F_2 folds are rare, and all of the early mesoscopic folds are tight to isoclinal. Large-scale F_1 folds are somewhat more common than F_2 folds and are generally of greater amplitude. F_1 and F_2 are more prevalent north of the structural style change boundary (marked SSC on Fig. 2). Extreme reorientation of all early structures makes determination of original fold vergence directions on Dutch Island impossible. The two fold generations are differentiated by the folding of S_1 by F_2 and by the presence of a new foliation (S_2) axial planar to F_2. The S_2 foliation is by far the most pervasive structural element on the island and is readily identifiable in all lithologies with the exception of the metaquartzite units. The attitude of S_2 is highly variable, because of the later deformation, but generally strikes N to NNE (Fig. 2). In the few northern areas unaffected by the later deformation, S_2 dips gently (6–20°) to the east. Elsewhere in the basin another foliation and associated phase of folding, formed during the early deformations, has been recognized and discriminated (Farrens 1982, Henderson & Mosher 1983, Reck 1985, Reck & Mosher 1989), but is not discernible on Dutch Island. F_1 and F_2 may be correlative with the basin-wide D_1 and D_2 events (Mosher 1983), respectively, or both may be part of D_1 that elsewhere in the basin was polyphase (Mosher 1985). The latter is most likely because elsewhere in the high-grade rocks of the southwestern basin, S_{1b}, a crenulation cleavage of S_{1a}, is the most pervasive foliation and S_2 is a less well-developed crenulation cleavage (Henderson & Mosher 1983, Mahler 1988, Reck & Mosher 1989). The intensity of the subsequent deformation (D_3–D_4) and the limited number of F_1 and F_2 structures remaining, makes it difficult to distinguish the two possibilities. In the following section the first two generations of structures will be referred to as F_1, S_1 and F_2, S_2 for simplicity although they probably are correlative to F_{1a}, S_{1a} and to F_{1b}, S_{1b} elsewhere in the basin.

The timing relationships between F_1, F_2 and M_1 (the first metamorphic event) and the structural complexity of the early deformation are best expressed in thin section. The S_1 foliation is a complex metamorphic foliation as shown by its expression in the metaconglomerates. Some pressure solution features are observed, such as quartz pressure shadows at the long axis terminations of larger quartzite cobbles, however, the interior of the cobbles show evidence of extensive intracrystalline plastic deformation. The S_1 foliation in the metapelites is defined by strongly aligned muscovite and biotite and is visibly transposed to form a crenulation cleavage, S_2. The more penetrative S_2 foliation is axial planar to microscopic F_2 folds, and micas that formed during D_1 are recrystallized in the S_2 crenulation hinges. The S_2 foliation wraps pre-existing garnet porphyroblasts and parallels quartz pressure shadows adjacent to the garnets. Quartz grains are generally elongate parallel to the S_2 foliation and have undergone significant recrystallization. In contrast, micas in D_3–D_4 crenulation fold hinges are not recrystallized, and no prograde minerals grew during D_3 and D_4.

The change from pressure solution to ductile deformation during F_1 and the growth of metamorphic minerals parallel to S_1 indicates that metamorphism began during F_1. In addition, the relationship between S_1 and S_2 foliations and the garnet porphyroblasts indicate that M_1 culminated near the end of F_1, prior to F_2. Finally, the presence of pressure shadows on garnets parallel to S_2, recrystallization of micas in S_2 crenulation hinges, and quartz deformation textures show that temperatures were still elevated during D_2, but were somewhat lower. The subsequent deformation apparently occurred at even lower temperatures.

A later retrograde metamorphic event (M_2) produced

randomly oriented chlorite grains, which were observed in all thin sections of Dutch Island rocks. Some chlorite grains are distinctly kinked by D_3 and D_4 events, whereas other grains show no evidence of deformation. This variation in chlorite deformation textures implies that chloritization occurred before, during, and after shear-related deformation. Elsewhere in the basin, however, the effects of retrograde metamorphism are localized along faults associated with D_3 and D_4 deformations (Henderson & Mosher 1983, Murray & Mosher 1984). Variable fluid migration along the faults, which were being reactivated at different times, would also produce the variation in chlorite deformation textures. In either case, the retrograde metamorphism resulted from an influx of fluids (Murray & Mosher 1984), not from an increase in temperature.

The end results of the deformation produced during initial closure of the Narragansett Basin was the formation of a near-perfect foliation (S_2), enhanced by high-grade metamorphism in all of the major lithologies. In areas unaffected by later deformation, this well-developed pervasive foliation is essentially planar with few perturbations, and nearly horizontal with a slight eastward dip. This orientation is consistent with that of the apparently correlative S_{1b} foliation found elsewhere in the basin away from shear zones. This foliation is not significant in itself, and can be found in greater or lesser degrees throughout the basin (Mosher 1976, Skehan & Murray 1979, Burks 1981, Thomas 1981, Farrens 1982, Mosher 1983, Reck & Mosher 1989). The presence of the foliation, however, combined with the generally fine-grained nature of the metasediments on Dutch Island, allowed remarkable preservation of later structures. Without the extremely well-developed pre-existing structural and metamorphic fabric preserved in the rocks, structures produced during later deformations would obliterate earlier structures and record only the most recent generation of significant deformation. Additionally, all subsequent structures are preserved because the later deformations occurred during the waning stages of metamorphism. The remainder of this paper will focus on the types of structures produced in a complex ductile shear zone and the implications that these structures have on the strain and kinematic history of Dutch Island and the Narragansett Basin.

Shear-related deformation

The majority of the observable deformation on Dutch Island may be attributed to discrete movement along a complex system of non-parallel, intersecting sinistral and dextral shear zones with approximately vertical shear planes. Structural superposition indicates that NNE-trending sinistral zones were first active, followed by dextral movement along predominantly NE- and then ENE-trending zones. Some shear zones presently in NE orientations underwent both sinistral and dextral movement, with sinistral motion always preceding dextral motion. Seven discrete fold generations were recognized and may be attributed to two progressive ductile shearing events on Dutch Island (D_3 and D_4). In addition, highly complex sets of discrete, incrementally-formed crenulation cleavages generated by strike-slip movement were preserved and remained distinct after as much as 44° of internal rotation. First we discuss the evidence that the observed structures result from strike-slip movement and demonstrate that they record the movement history. Then we describe the specific structures observed in the area and the resulting conclusions.

Evidence for strike-slip motion and movement history

Faults and shear zones. Discrete vertical strike- and oblique-slip faults and shear zones (with widths varying from 0.6 to 20 m and indeterminate lengths) were mapped on Dutch Island (Figs. 2 and 3). Those faults and zones oriented NNE to NE show measurable offset or kinematic indicators indicating sinistral motion and those oriented NE to ENE show dextral motion. The most intense deformation is observed where zones intersect (i.e. in the southern part of the island) or within NE-trending shear zones that have undergone both senses of motion.

On the northern part of the island (north of the SSC

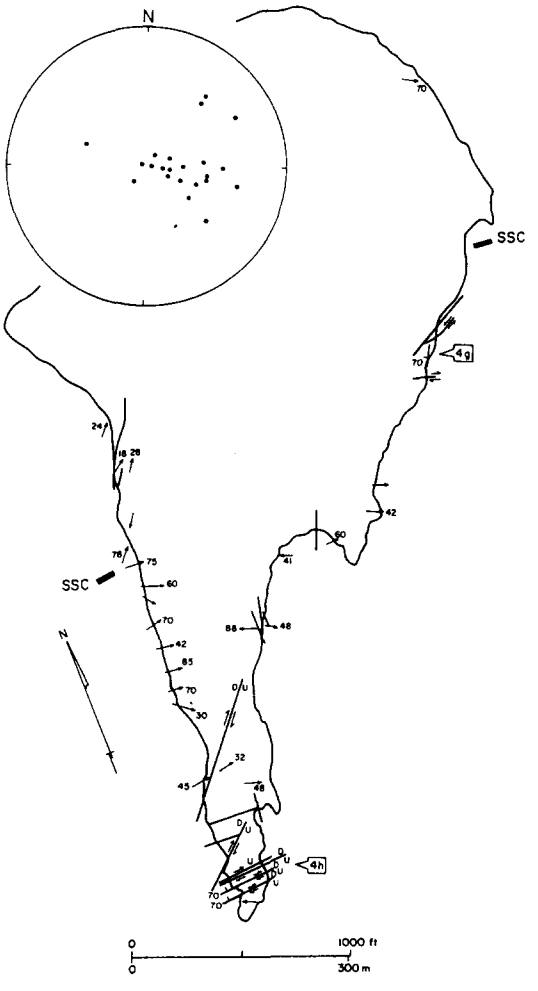

Fig. 3. Map showing location of measurable brittle faults and stereoplot of slickenside lineations. Except where noted, faults are vertical. Minor faults shown by slickenside lineations, which parallel fault trends. Movement on major faults shown only where offset can be measured. Locations of Fig. 4(g) & (h) shown.

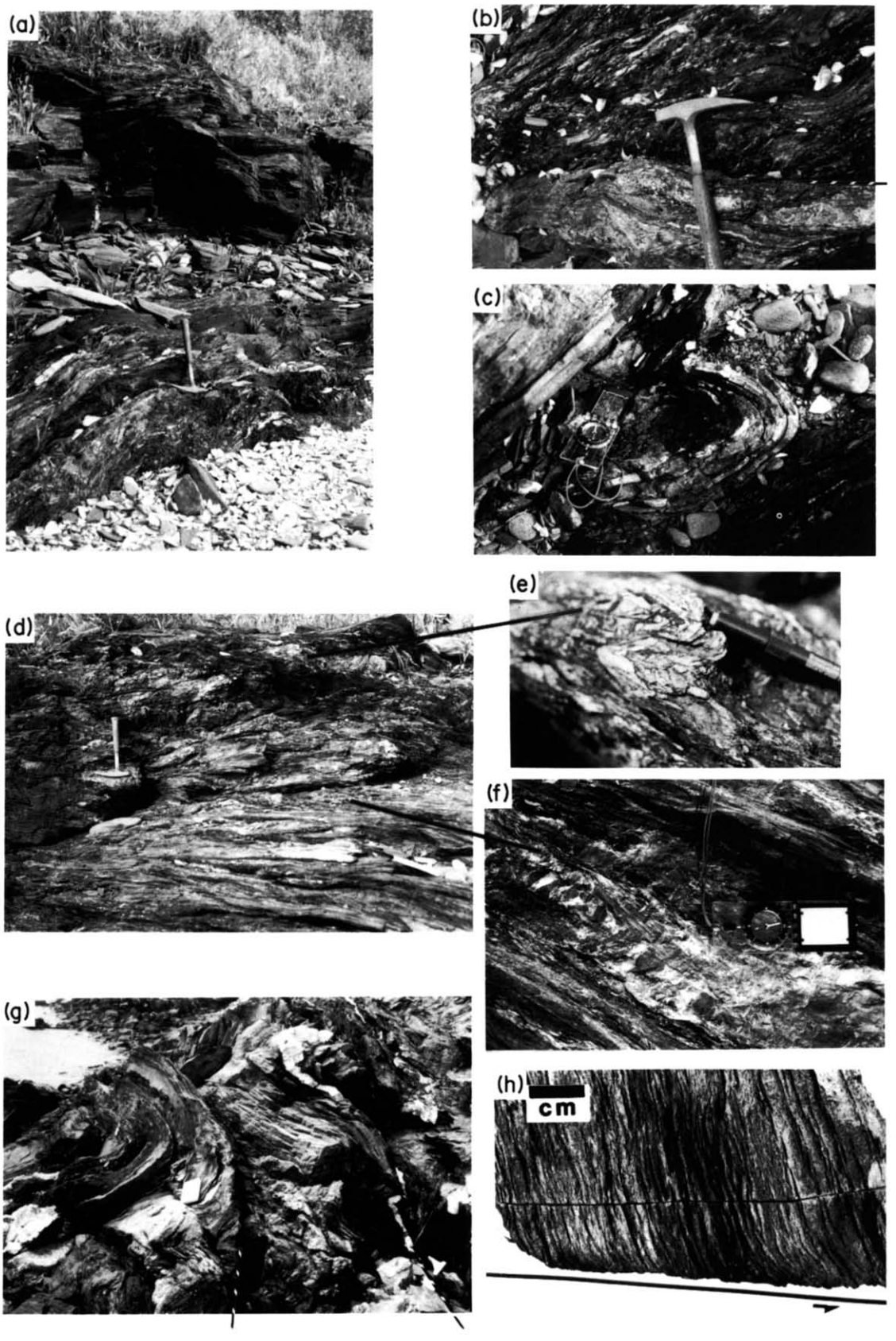

Fig. 4. Discrete, ductile shear zones, faults, and associated structures. See text for discussion. Locations given on Figs. 2 and 3. Traces of late brittle faults marked by dashed lines at one end. (a) Highly-sheared, vertical zone. Note difference in orientation between foliation in zone and surrounding rock. (b) Close-up of foliation within zone in (a). (c) F_5 fold trending S60°E, plunging 78°S within discrete shear zone. (d) Vertical shear zone. Note folds of the shear-related foliation in upper left. (e) Close-up of one fold in (d). (f) Close-up of part of zone in (d) showing fibers connecting blocks of foliated, pulled-apart phyllite. (g) Pervasive F_5 and F_6 folds cut by later brittle faults. (h) Hand sample taken adjacent to minor, ENE-trending, vertical fault (trace shown by line). Shear direction (shown by arrow) lies in plane of photograph and in field, plunges steeply east.

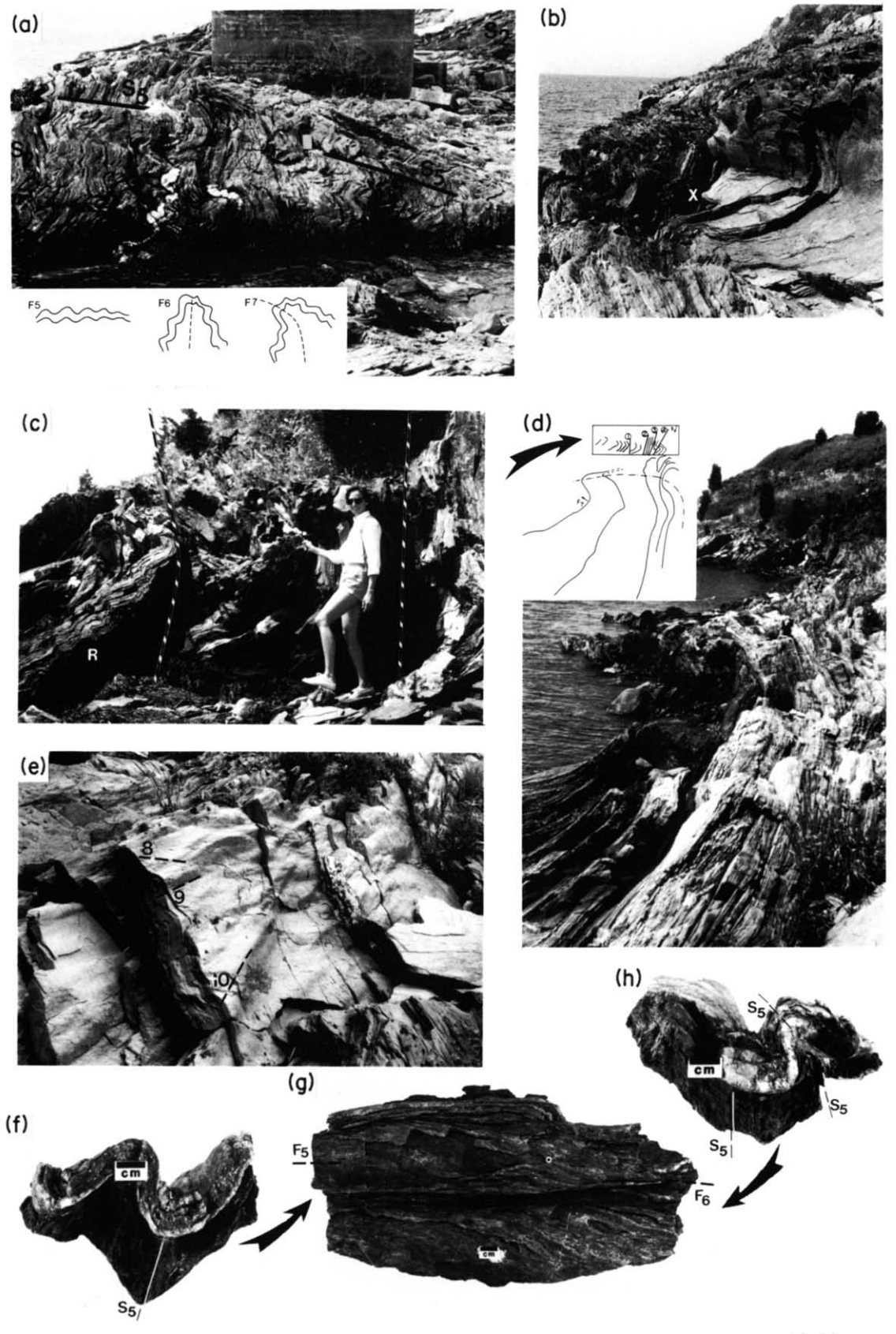

Fig. 5. Multiple generations of shear-related folds. See text for discussion. Locations shown on Figs. 9 and 12. (a)–(d) Taken looking south; (e) looking north. (a) Relationship between F_5, F_6 and F_7. F_5 chevron fold-axial planes (labeled S_5, solid lines) broadly warped by F_7 folds; recumbent appearance of the F_6 fold (defined by folded S_2, see dashed lines) results from refolding on oblique open F_7 axis. Sketch shows sequence of fold formation. (b) Overturned F_6 folds folded by oblique F_7 fold; F_6 syncline has little plunge. F_6 anticline plunges moderately south; accommodation fold on the intervening limb (to right of X). ENE-trending fault cuts structures (nearly parallel to the plane of the photograph; connect dashed lines. X lies on fault plane); no ductile reorientation of structures adjacent to fault. (c) Dextral shear-related folds (at R) on moderately E-dipping F_6 fold limb. Vertical faults 1 (NNE trend) and 2 (NE trend) from sketch in (d) are shown (dashed lines) (see Fig. 3). A third fault (parallel to plane of photograph) exposed in upper right; arrow parallels slickensides. (d) F_6 fold refolded by F_7 as shown in sketch (a). (Sketch of outcrop: dash-dot line is F_6 axial plane.) View in distance same as in (c).

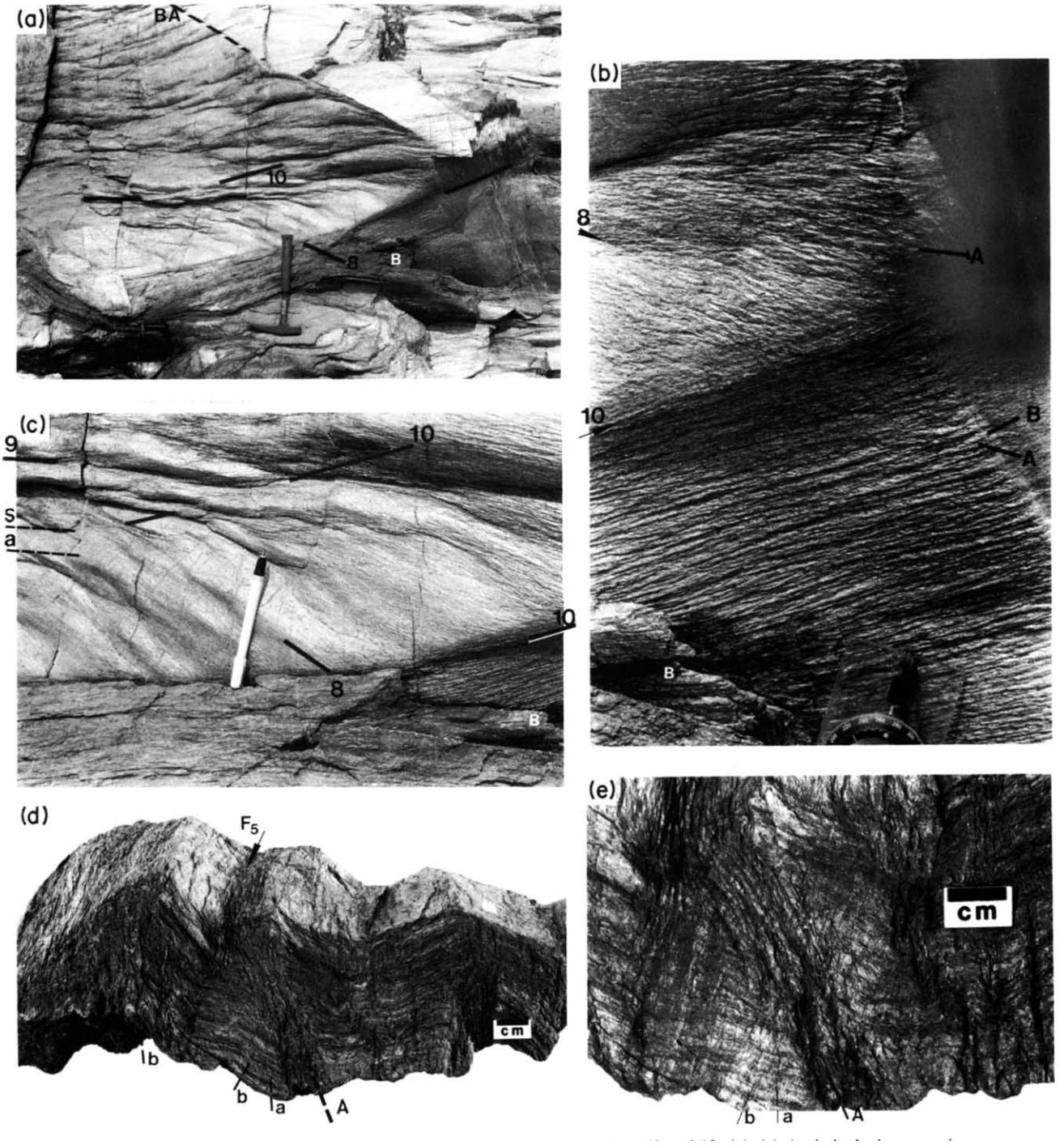

Fig. 7. Crenulation cleavages and late structures. Locations shown on Figs. 10 and 12. (a)–(c) Anti-clockwise-younging F_8–F_{10} folds and generally non-coaxial superposed crenulations. (c) is close-up of area above hammer handle in (a); (b) is a close-up of right side of (a) and (c)—the white B is in same location in all three photographs. All views to west. (a) View of E-dipping S_2 surface folded by cross-cutting F_8–F_{10} folds and warped by late-stage boudinage. Inverse view of 'dimple-like', N60°E-trending boudin neck (BA, dashed line at one end). East-striking tension gashes and conjugate kink bands are visible also in (c). (b) Cross-cutting crenulation cleavages with anti-clockwise-younging direction. A is clearly crenulated by B. (c) Close-up showing F_9 antiform (a), synform (s) pairs interfering with F_8 folds. F_8 axes in lower right curve around F_{10} fold. (d) & (e) Hand sample of superposed crenulations on S_2 surface folded by F_5 chevron folds. Cleavages a and b show clockwise-younging; cleavage A is related to dextral shear. Sample field orientation: limb on right side of labeled F_5 axis is horizontal, cleavage a and b dip west, A is vertical. (d) Cross-sectional view of crenulation A cross-cutting a and b. Note that A only formed on F_5 fold limbs that were horizontal in the field, not on steeply E-dipping limbs. Cleavage b appears nearly axial planar with F_5; divergence between b cleavages caused by later unfolding of F_5 synform. On right, b forms an en échelon pattern. Cleavage a is barely visible. (e) Looking down on labeled surface in (d). Cleavage b cross-cuts a faint a; both are cut by A.

Fig. 5 (*cont.*) ENE-trending fault plane (shown as rectangle on sketch) cuts through cove; faults 3 and 4 trend NE similar to fault 2. (e) Anti-clockwise-younging, doubly plunging, 'ripple-like' F_8, F_9 and F_{10} folds on a moderately E-dipping surface. (f)–(h) Hand sample of F_5 fold (of S_2) modified by later F_6 fold at slightly oblique angle. A quartz vein parallels S_2 on upper part of sample. In field, enveloping surface of folds—N20°E 90°; S_5 shallow west dip. (f) & (h) Cross-sectional views of opposite ends of sample. (g) Plan view; note rounded F_5 changes trend slightly and becomes tighter to right where it has become an F_6 fold (i.e. folds S_5).

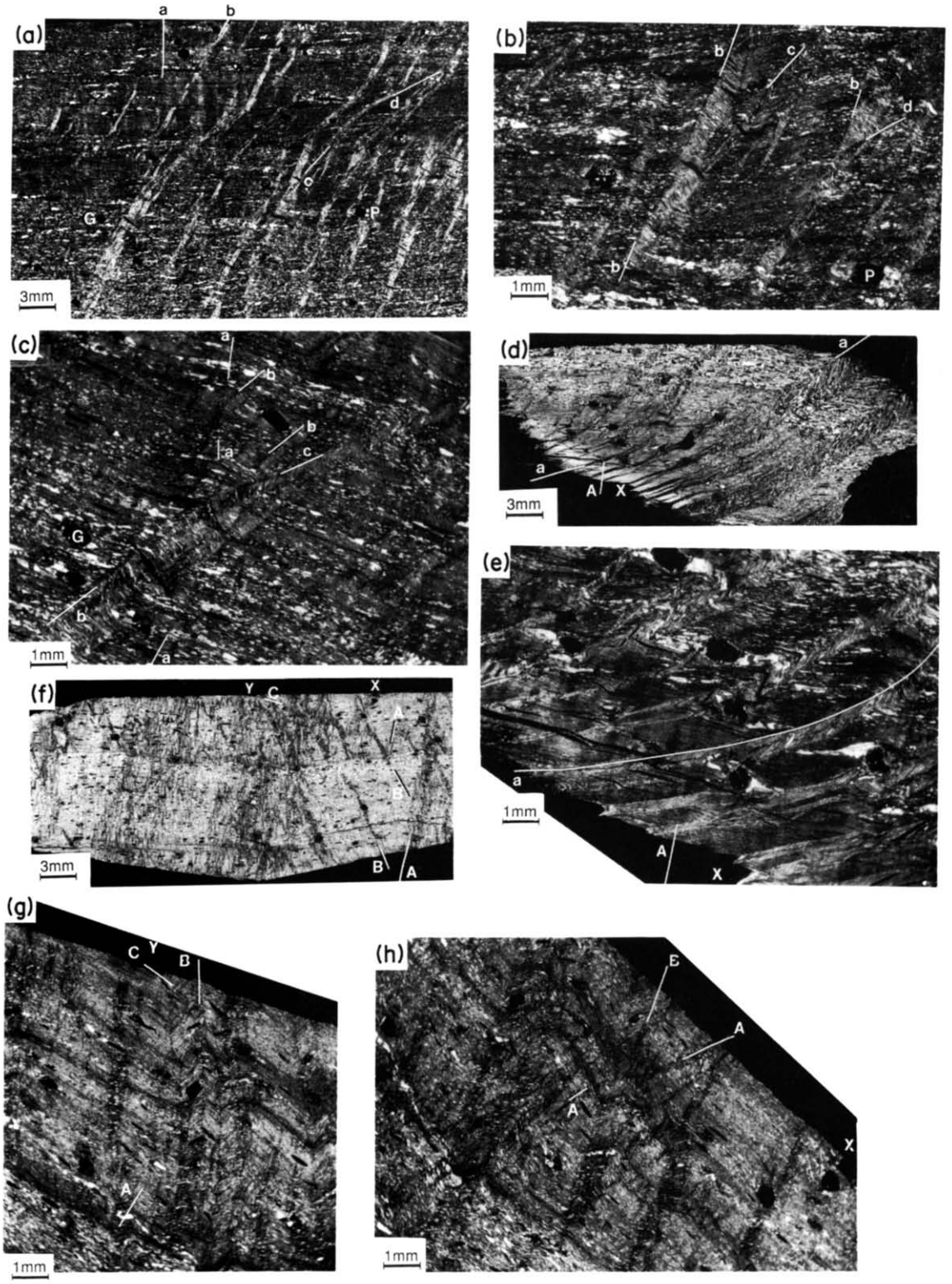

Fig. 8. Photomicrographs of superposed crenulation cleavages. Sample locations shown on Fig. 10. In most examples only one cleavage of each generation is marked, other parallel cleavages are of same generation. (a) Entire thin section showing clockwise-younging cleavages (a—oldest, d—youngest). Cleavages b, c and d are en échelon. Where d crosses cleavage b, b crenulations appear to be bent. (P and G refer to similar points in close-ups in b and c.) This section taken from a presently vertical limb of F_5 fold (from area shown in Fig. 5a); cleavage a formed before F_5 folding, b is nearly axial planar, c and d formed after F_5 and F_6 folding. Section orientation: N70°E 90°; up to right, east to top. (b) Close-up of area around P in (a). Cleavage b is crenulated by c; cleavage d only shows up on one limb of b. (c) Close-up of area around G in (a). Cleavage a can be traced through b crenulation and is folded by it. Cleavage c cuts across and merges with b. (d) F_5 fold with axial planar cleavage a gently folded by F_7 fold. Later dextral shear-related cleavage A is labeled. Section orientation: E–W 90°; up to top, east to right. (e) Close-up of area near X marked in (d). Cleavage A is only observed on one limb of a cleavages. (f) Anti-clockwise younging crenulation cleavages. En échelon B cleavages cross-cut A; C not visible on this scale. (X and Y areas marked on close-ups in g and h.) Section orientation: N50°W 90; up towards bottom left; east to left. When reoriented to field position, cleavage A—vertical, C—horizontal. (g) Close-up of area around Y in (f). Cleavage C is tight crenulation that only affects one limb of the B cleavage. (h) Close-up of area to left of X in (f). Individual A cleavages can be traced through B crenulations and are folded by them.

boundary) shear zones are discrete and contain shear-related structures not observable outside the zones. Discrete shear zones are best expressed on the northwest side of the island in a graphitic black phyllite (Fig. 4). These highly sheared zones are generally vertical and trend N18°E (Fig. 4a) to N27°E (Figs. 4c & d). Parallel faults undulate and appear to be gently folded or warped on an E-trending axis. The zones are 0.6 m wide and alternate with coarse, sandy black phyllite (Fig. 4a). Although these northwestern zones are concentrated in the graphitic phyllites, they widen and involve other units southwards toward the SSC boundary. Within these zones the foliation is more closely spaced and better defined and represents either a new shear-related foliation or an enhanced S_2 (Fig. 4b). This foliation is tightly folded by folds not observed outside the zone (Figs. 4d & e), and folds observed outside the zone are reoriented within the zone (Fig. 4c). Discrete shear planes within the zones are defined by blocks of phyllite that have been pulled apart and are connected with fibrous quartz (Fig. 4f).

The discrete zones on both sides of the island become wider and more closely spaced southwards approaching the structural style change (SSC) boundary. South of the boundary, the shear-related deformation is so pervasive that discrete shear zones responsible for this deformation are difficult to delineate. In this area, however, the pervasive shear-related structures are cut by discrete zones of more intense and complex deformation, and the pre-existing shear-related structures swing into parallelism with these zones. Additionally, many major shear zones (and faults?) can be inferred on the island. These zones were marked by a break in outcrop and a topographic lineament. Approaching these breaks, the magnitude and intensity of the shear-related deformation increases although the style of deformation does not change. In most cases, shear-related structures swing into parallelism with the topographic lineaments. These inferred shear zones and the mapped major zones are shown on Fig. 2 and all future maps (other than Fig. 3) as solid lines. Minor zones have been omitted for clarity.

Many brittle faults were readily measured in outcrop (e.g. Figs. 4b, c & g) and are shown in Fig. 3. Except where the dip is given, faults are essentially vertical although most undulate somewhat (±10° of vertical). Major faults are indicated by solid lines with motion shown only where offset is measurable. These faults are predominantly dextral with a vertical component of motion and are most abundant in the south. All occur within major shear zones and parallel the shear zone boundaries. Although motion cannot be determined on many faults, where it can be determined, the faults show the same sense of motion as kinematic indicators in the adjacent shear zones. The shear zones associated with the ENE-trending major faults are narrower and more discrete than those associated with NNE- and NE-trending faults. The major faults clearly post-date most, if not all, of the ductile strain within those zones. For example, the shear-related folds in Fig. 4(g) are clearly cut by a brittle fault and show no apparent genetic relationship to the fault (e.g. 'drag' folds).

Most faults are minor, however, and show slickenside lineations (e.g. Fig. 5c). Only the lineation is plotted on Fig. 3 because the faults are vertical and the trend of the lineation parallels the trend of the fault. All of these faults show oblique-slip motion. The majority of faults with slickensides are nearly E-trending with a few NE-trending ones; none trend NNE (Fig. 3). The minor E-trending faults cut all structures (e.g. Fig. 5b) and are bounded by narrow zones (0.5–5 cm) of ductilely reoriented structures (Fig. 4h) that indicate the same sense of motion as the faults where offset can be determined. These narrow zones could have formed synchronously with the faults or these faults, like the major faults, could represent the last stages of shearing. All ENE-trending faults with measurable offset are dextral; most show vertical motion with up to the south. If the E-trending faults with slickensides are also dextral, these oblique-slip faults also indicate up to the south. The narrow width of the shear zones associated with the E-trending faults and the abundance of slickensides on these faults, when compared with the wider zones and lack of slickensides on NNE-trending faults and lesser number on NE-trending faults, suggest that conditions were most favorable for brittle deformation during movement on E-trending zones and for ductile deformation during movement on NNE- and NE-trending zones.

Kinematic indicators. Many types of kinematic indicators are present within the shear zones such as sheath folds, en échelon folds and tension gashes. Within major zones, small-scale subsidiary shear zones with boundaries parallel to the major zones show measurable ductile offsets of structures that clearly show the sense of shear. Also, structures outside shear zones can be traced into the zones, and these structures gradually change orientation until they lie parallel or nearly parallel to the shear plane, again indicating the sense of shear. All of these features allow the sense of shear for the shear zones on Dutch Island to be determined. However, on this island, multiple generations of folds and crenulation cleavages formed within the shear zones, and their superposition and consistent younging direction provides unusual and accurate kinematic indicators. These structures and a model for their formation will be discussed below, and specific examples using these folds and cleavages as kinematic indicators will be provided in later sections.

Adjacent to major faults and within shear zones, several generations of post-F_2 folds are observed. These fold generations are non-coaxial and show consistent cross-cutting relationships. The earlier folds are progressively tightened, and the axial surface and axes of the earlier folds are folded by the subsequent folds in the set (Fig. 5). These relationships show that each fold within the set is a discrete fold generation. Several factors indicate that a shear couple caused successive folds to form at an oblique angle to the shear plane and to rotate toward the shear plane where they were sub-

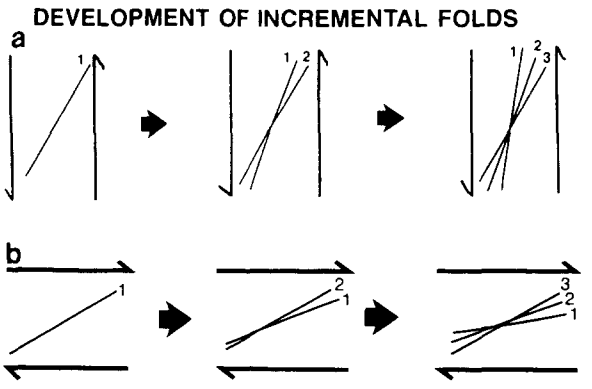

Fig. 6. Schematic diagram showing development of incrementally formed folds within a simple shear system. Layering (S_2) is horizontal (within plane of page) and shear zone is vertical (perpendicular to page). Fold axes numbered in order of formation (1—oldest, 3—youngest). (a) Sinistral system. (b) Dextral system.

sequently overprinted by further folds in the set: (1) shear zones are essentially vertical, and other independent kinematic indicators show oblique- or strike-slip sense of motion; (2) the S_2 foliation is nearly horizontal outside the shear zones both on Dutch Island and elsewhere (S_{1b}) in the southwestern basin; (3) the angle between individual folds in a set are small, and folds have little to no plunge; (4) the folds within a set show a uniform younging direction (either clockwise or anti-clockwise); and (5) the sense of shear indicated by these superposed folds matches that given by independent kinematic indicators in all cases.

The formation and internal geometry of the post-F_2 folds can be explained by the following model: vertical shear zones undergo strike-slip movement. Because S_2 is nearly horizontal (i.e. perpendicular to the shear plane but parallel to the kinematic *a* direction), the shear strain is accommodated by formation of a generation of folds at an oblique angle to the shear plane. As movement continues along the shear zone, the newly formed fold generation will be rotated toward the kinematic *a* direction (Ramsay 1980, Skjernaa 1980) and thus closer to parallelism with the shear plane. As movement and subsequent rotation continues, strain within the *XZ* plane tends to tighten the pre-existing folds so that earlier fold generations have smaller inter-limb angles than younger folds. Structures of this nature may form within either a transpressional or a simple shear system, illustrated in Fig. 6(a). In this example, fold 1 forms within a sinistral shear couple by flexural-slip and is rotated and tightened until flexural-slip can no longer occur. Fold 2 then forms at an angle to the shear plane, overprinting 1, which is now essentially locked because it can no longer accommodate the strain. Internal rotation of both 1 and 2 continues until 2 can no longer accommodate the strain, at which point fold 3 is formed, overprinting both pre-existing fold generations. Note that this anti-clockwise rotation of folds produces clockwise younging folds. Figure 6(b) shows the same sequence of events but for a dextral shear couple. In this case, clockwise rotation of folds produces anti-clockwise younging folds. In either case, several generations of superposed folds form as the result of continuous movement during a progressive deformation. With increasing displacement, the centers of the zones undergo the most strain, and, when coupled with strain hardening, an increase in strain rate, decreasing temperatures, or larger displacements, faults form. Thus the movement history of individual shear zones on Dutch Island can be determined using the post-F_2 fold sets.

Perhaps the most accurate means of determining the detailed movement history for shear zones on Dutch Island is the measurement and geometric analysis of multiple generations of superposed crenulation cleavages. These cleavages are non-coplanar, and the lineations on S_2 are non-coaxial. The angles between cleavage and lineation generations is small, ranging from 4 to 22°. The cleavages are not conjugate sets and show consistent cross-cutting relationships (Figs. 7 and 8). The cleavages are found in the same shear zones as the superposed mesoscopic folds but are rarely axial planar to the folds (Figs. 7d and 8d). Overprinting relationships between crenulation cleavages are consistent and show either a clockwise or anti-clockwise younging which matches that of the mesoscopic folds in the same zone. North of the SSC boundary, cleavages are found only in discrete shear zones, whereas south of the boundary, the cleavages are pervasive, but increase in number as cross-cutting shear zones and zone intersections are approached, reaching a maximum of eight generations of superposed crenulation cleavages (excluding S_2) on the southern end of the island. Even at the southern end of the island, individual cleavages can be traced laterally in continuous outcrop for tens of meters. The above relationships indicate that these consistently younging crenulation cleavages formed incrementally in response to a shear couple in the same manner as discussed for the mesoscopic folds, just on a smaller scale. Detailed analysis of these cleavages therefore allows accurate tracking of movement within shear zones with time.

Crenulation cleavage geometries were studied in the field, in handsample, and in over 100 oriented thin sections from samples taken from both within and between shear zones. All generations of crenulation cleavages associated with strike-slip deformation fold the S_2 foliation. Clear crenulation cleavage superpositions were evident in the majority of thin sections examined (Fig. 8). Types of overprinting relationships range from microfolding of the earlier crenulation by the later one to the formation of the later crenulation on only one limb of the earlier one because the other limb was in an inappropriate orientation. Several examples are given in Fig. 8 and are discussed in detail in later sections. Unlike the shear-related folds, no relationship between age and tightness of crenulations was observed. Additional crenulation cleavages that nucleated off pre-existing garnet porphyroblasts were observed in some thin sections, however, the new cleavages merged together into one cleavage parallel to the rest within a distance approximately equal to the diameter of the porphyroblast. In many thin sections, crenulation cleavages were not con-

tinuous across the length of the section. Instead, parallel cleavages were en échelon with one starting where another left off (Fig. 8a). Such en échelon arrays in cross-section were rarely seen in hand sample (Fig. 7d). In summary, major generations of crenulation cleavages with consistent orientations were easily discernible in the field, and overprinting relationships could be confirmed in thin sections.

The crenulation cleavage data was most useful for structural analysis within shear zones that underwent both senses of shear and in areas of limited or poor quality outcrop. Cleavages were useful because a large amount of data could be collected in a relatively small area and overprinting relationships between sinistral and dextral crenulation cleavages were usually easier to document than those between sinistral and dextral folds. The statistical dependability of crenulation cleavage internal geometries allowed for structural interpretation of sporadic outcrop along heavily vegetated or otherwise unexposed shear zone traces. In all cases, crenulation cleavage data corroborated the movement history documented by superposed mesoscopic fold generations and other independent kinematic indicators. The kinematic interpretation of the multiple generations of non-coaxial crenulation cleavages formed during progressive deformation is much the same as was described for larger structures. In short, a clockwise younging direction in a set of crenulation cleavages indicates anti-clockwise internal rotation and sinistral shear. Conversely, anti-clockwise younging directions of crenulation cleavages indicate clockwise internal rotation and dextral shear. The orientations of the youngest cleavages, combined with the principle that rotated structures may approach but not lie parallel to the shear plane, help determine the orientation of the original shear plane in areas where shear zone boundaries are not exposed or cannot be measured. For shear strains calculated using these cleavages on Dutch Island and elsewhere in the basin, see Burks (1985).

SINISTRAL SHEAR INDICATORS

Shear zones mapped on Dutch Island that trend NNE to NE contain kinematic indicators indicative of sinistral strike-slip movement. These indicators include reorientation of structures present outside the shear zones into near parallelism with the shear plane within the zones, smaller-scale, subsidiary shear zones that show ductile offsets and en échelon folds. Superposed mesoscopic fold and crenulation cleavage geometries on the island also indicate sinistral strike-slip movement on shear zones with these orientations.

Three distinctly different superposed fold generations (F_5, F_6 and F_7) may be attributed to sinistral strike-slip movement (fold generations F_3 and F_4 are preserved as highly reoriented structures and are discussed later). These folds formed almost entirely by flexural-slip along the well-developed S_2 foliation planes. These folds consistently young in a clockwise manner according to Fig. 6(a), (Fig. 9), and may be briefly characterized as follows.

F_5: Open to tight, chevron folds. These folds may be upright, recumbent or downward-facing and have an average amplitude of 2–10 cm. Interlimb angles range from 47 to 84° with an average angle of 64°.

F_6: Open to tight, upright to recumbent folds. The folds verge eastward and range in amplitude from 15 cm to >5 m. Interlimb angles range from 87 to 121° with an average angle of 104°.

F_7: Extremely broad, upright folds. The axes of these folds are best defined by mapping the reorientation of F_5 and F_6 axes and axial planes. Interlimb angles range from 145 to 171° with an average angle of 164°.

The field relationships between these fold generations are readily visible in outcrop. For example, Fig. 5(a) shows S10°W-trending, F_5 chevron folds folded about

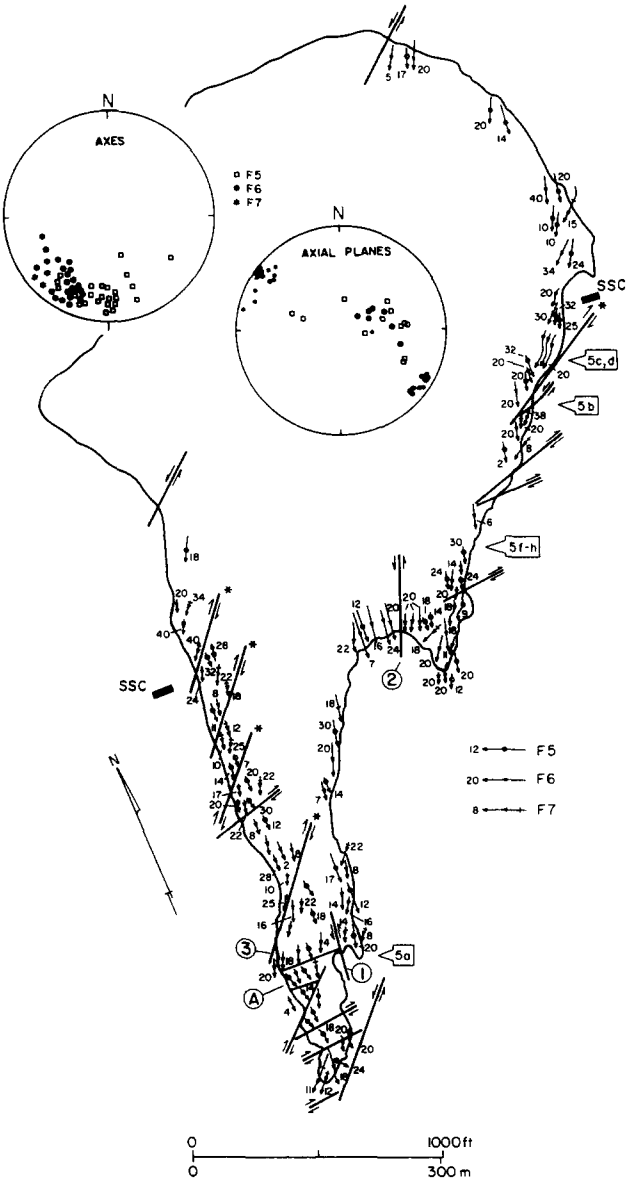

Fig. 9. Structural map of major F_5, F_6 and F_7 folds and stereoplots of fold axes and poles to axial planes. Fold axes plunges on map indicated in degrees. See text for discussion. The twisted fold axes are caused by large, SW-plunging F_7 folds (axes not shown; for example, see Fig. 5d). (For shear zones 1 and 2, see Table 1; area A discussed in text.) Locations for Fig. 5 shown.

Table 1. Fold orientations within sinistral and dextral shear zones of different orientations

(A) Sinistral shear zones		
Shear zone orientations	Fault 1—N8°E	Fault 2—N20°E
Fold orientations		
F_5	S12°W, 20°S	S21°W, 14°S
F_6	S20°W, 14°S	S30°W, 10°S
F_7	S38°W, 14°S	S46°W, 6°S
Angle between folds (in degrees)		
F_5 and F_6	10	11
F_6 and F_7	18	17
F_5 and F_7	28	30
Angle between folds and shear plane		
F_5	4	1
F_6	12	10
F_7	30	26
(B) Dextral shear zones		
Shear zone orientations	Fault 4—N52°E	Fault 5—N74°E
Fault orientations		
F_8	S44°W, 6°S	S50°W, 4°S
F_9	S32°W, 9°S	S40°W, 10°S
F_{10}	S24°W, 8°S	S30°W, 12°S
F_{11}	S18°W, 14°S	S25°W, 10°S
Angle between folds (in degrees)		
F_8 and F_9	12	12
F_9 and F_{10}	8	10
F_{10} and F_{11}	6	5
Angle between folds and shear plane		
F_8	8	24
F_9	29	34
F_{10}	26	44
F_{11}	32	49

the S20°W-trending axis of a presently recumbent F_6. Both of these fold generations are broadly warped about a S40°W-plunging F_7 fold axis. Recumbent and downward-facing folds form because the scale of these non-coaxial folds generally increases from F_5 to F_7 and the difference in scale between F_5 and large F_6 folds is much greater than that between F_7 and large F_6 folds. F_5 folds are recumbent on the limbs of much larger F_6 folds (see Fig. 5a sketch). The large F_6 folds change from upright to recumbent along strike as they are folded around the hinges of F_7 fold (Figs. 5a & d). This folding of F_6 by F_7 results in downward-facing F_5 folds on the overturned limbs of recumbent F_6 folds. The evolution of these folds is sketched in Fig. 5(a). Note that the axial planes of F_6 folds are only folded into recumbent folds in the hinges of F_7 folds where the two non-coaxial folds intersect. Thus, the F_6 and F_7 sketches (Fig. 5a) are also equivalent to serial cross-sections along the length of a F_6 fold; the sketch labeled F_6 is of F_6 away from F_7 hinges, and the one labeled F_7 is F_6 at the intersection of the two folds.

The orientation of fold axes are also affected by the subsequent fold generation, causing trends and plunges of individual folds to vary along strike. This refolding occurs along an axis that is at a small angle to the previous fold axis. For example, F_6 and F_7 axes usually are at an angle of ~20° to each other (see Table 1 and Fig. 9). When both F_6 and F_7 are broad folds, resultant folds of one limb of the F_6 folds may have very different trends and plunges than those of the F_6 axial planes and the other F_6 limb. For example in Fig. 5(d), the F_7 fold axis on the left limb of the F_6 fold plunges SE (see sketch), oblique to the general SW plunge of F_7 folds of F_5 and F_6 axial planes. This refolding of F_6s by F_7s results in the twisted axial traces shown on Fig. 9. Also, folds in uncharacteristic orientations that die out along strike may form on one limb of F_6 folds to accommodate the change in plunge of the F_6 folds caused by an oblique F_7 fold (Fig. 5b).

The angular relationship between F_5 and F_6 is usually smaller (~10°, see Table 1 and Fig. 9). When folds are of equivalent sizes, distinguishing the generations is more difficult. For example, the antiformal axis indicated on the hand sample in Fig. 5(g) apears to be one fold generation that changes orientation along its trend by about 10°. This antiform is an F_5 fold that has been modified by an F_6 fold. A cross-sectional view through one end shows an upright, open F_5 fold with an axial-planar crenulation cleavage (Fig. 5f). At the opposite end of this antiformal axis, the cross-sectional view shows the crenulation cleavage is folded by this antiform that here is a tight, overturned fold (Fig. 5h). The antiform at this end must be a younger generation structure (F_6) because the S_5 cleavage is folded by it. The change in trend of the antiform axis (Fig. 5g) occurs where the F_6 fold starts (i.e. where S_5 becomes folded). Rather than producing an entirely new fold, the already present F_5 fold was modified on one end to become an F_6 fold.

The angular relationship between these three fold generations is well expressed on stereoplots of major and minor fold axes and axial planes (Fig. 9). F_7 axial planes are generally NE-striking, upright and unfolded. F_6 axial planes are folded somewhat on SW-plunging axes (F_7 folds). The F_5 axial planes are clearly folded, but the poles to the planes do not fall in a single great circle girdle. The distribution is best explained by folding on SSW- (F_6) and SW-plunging (F_7) axes. Fold axes of all three generations are somewhat variable in orientation, as would be expected, because earlier generations are refolded and later ones formed on previously folded surfaces. Additionally, fold orientations are variable depending on shear zone orientations (see Table 1), and some folds have been reoriented by dextral shearing. Nevertheless, the internal geometry between fold generations is consistent and younging is consistently clockwise.

The consistency of the younging direction and internal geometry of these folds is best shown on the map in Fig. 9. On this map, only large-scale folds are shown. Where only one generation is shown, age was determined by superposition relative to small-scale folds or rarely style. For example, in the northwest, F_7 folds are very broad, upright folds, some of which fold smaller-scale F_5 and F_6 folds. Note that folds everywhere young in a clockwise direction. Even where axes are twisted because of subsequent folding or deflected by later dextral shearing, this internal geometry is maintained.

The F_5–F_7 folds increase in number and size southwards on the island. North of the structural style change boundary (SSC), these folds are found in discrete, narrow shear zones that trend N to NNE. South of this boundary, these folds are pervasive and individual sinistral shear zones (with the exception of those that show both motions) usually cannot be identified. The orientations of the folds suggest that the zones causing the pervasive folds trend N to NNE, and rare major zones (1 and 2 on Fig. 9) south of the SSC boundary also show these orientations. Some NE-trending zones that show dextral motion are thought to also show early sinistral motion (marked with an *) because F_5–F_7 folds (and early generations of crenulation cleavages) increase in magnitude and number approaching these zones. The orientations of the folds are incorrect for sinistral motion on these zones (i.e. fold axis trends should be counterclockwise from the shear plane), however, suggesting that these were originally NNE-trending zones that have been partially rotated toward a NE-trend along with the sinistral structures during dextral shearing. Location and orientation of the sinistral shear zone boundaries are obscured by the late dextral shearing. Although these apparently rotated zones could be responsible for the pervasive F_5–F_7 folds found south of the SSC boundary, it is equally likely that NNE- or N-trending zones occur offshore and possibly in the island's interior parallel to the outcrop trend.

In summary, the superposed mesoscopic fold generations F_5, F_6 and F_7 provide an excellent kinematic indicator that is consistent with other more conventional indicators. Progressive tightening of limbs of earlier folds as well as consistent cross-cutting relationships among these fold generations indicates that they are discrete fold generations. These folds deform S_2, which is nearly horizontal away from the zones, and are found in nearly vertical shear zones. The uniform clockwise younging directions of these folds and the small angle between fold generations suggest that successive folds formed and were then rotated in an anti-clockwise manner. This motion is consistent with what is expected within a sinistral shear couple which underwent progressive movement. An average of 8–11° of anti-clockwise internal rotation was measured between F_5 and F_6, and 16–20° of rotation between F_6 and F_7. Incremental fold orientation data for two sinistral shear zones, a N- and a NNE-trending one, are summarized in Table 1. Angles between the shear plane and individual fold generations show that F_5 folds have been rotated approximately parallel to the shear plane, and that F_7 folds are at about a 30° angle to that plane, suggesting that the folds may have formed at a slightly greater angle to the respective shear planes. The overall similarities of fold morphologies for individual fold generations may also suggest that strain rates along strike-slip zones were fairly homogeneous during this deformation despite differences in zones orientations.

Geometric analysis of crenulation cleavages and lineations on the S_2 surface indicates that NNE- and some NE-trending shear zones show a sinistral shear sense, consistent with other kinematic indicators including superposed, mesoscopic fold data. Clockwise-younging crenulation cleavages are found across the entire island (Fig. 10), although they intensify approaching NNE- and some NE-trending shear zones. Four clockwise-younging crenulation cleavage generations are found on the island. All four are not present everywhere, but generally three generations can be identified (Fig. 10). The first three cleavages (a–c) are the most abundant, except on the southern tip of the island where the last cleavage (d) is dominant. Elsewhere the (d) lineation is relatively common, but the cleavage, itself, is absent. In thin section, the earlier cleavages can usually be traced through the cross-cutting younger ones and are

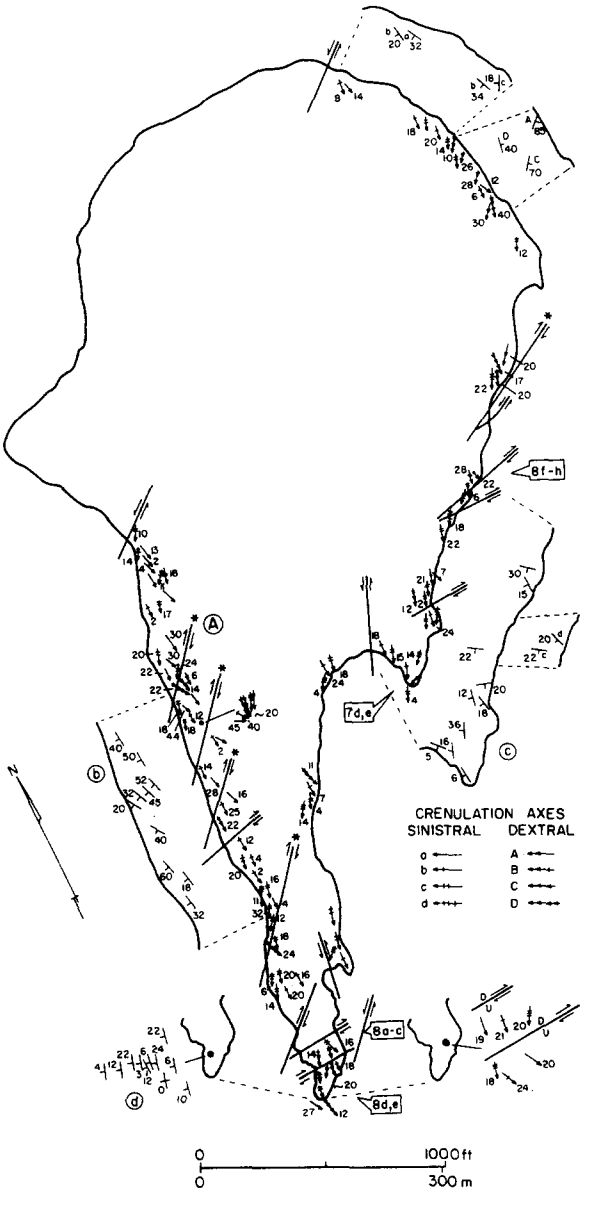

Fig. 10. Structural map showing crenulation cleavage generations (a—oldest sinistral, A—oldest dextral; dextral postdates sinistral). Complete map shows crenulation axes; pull-outs of coastline show strike and dips of cleavages. Large pull-outs labeled b, c and d show cleavages of that generation; note that these generations are folded. Pull-out b—most major folds here are S-plunging F_6 and F_7; pull-out d—shallow, late d cleavage is gently folded by broad F_7 folds; pull-out c shows effects over a large area of several SW-plunging F_7 folds. Pull-out map of lineations (southern end of island) and area A discussed in text. Locations for Figs. 7 and 8 shown.

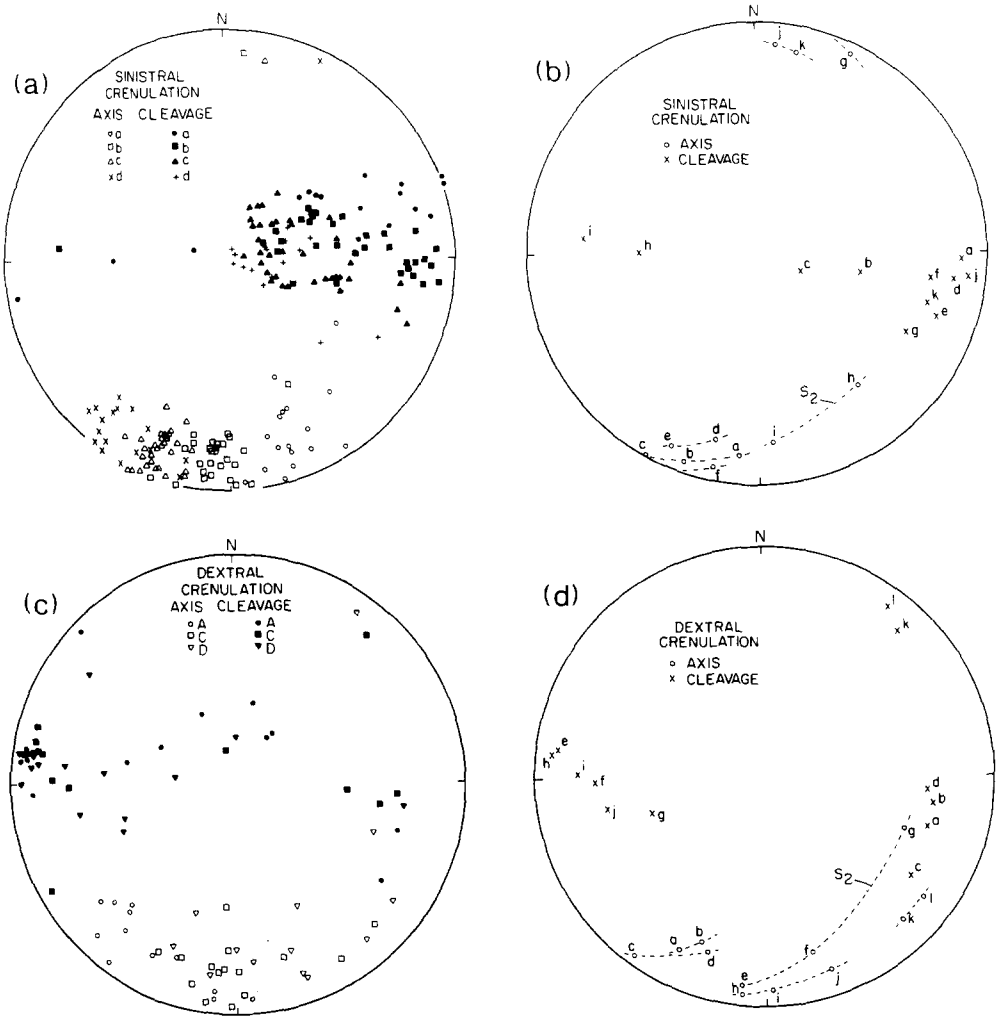

Fig. 11. Stereoplots of crenulation axes and poles to crenulation cleavages. (a) Clockwise younging crenulation lineations (a—oldest; d—youngest). Poles to cleavages show all folded with d folded the least and a the most. Poles to c and d fall on diffuse girdles around SW-plunging axes (F_7 folds), whereas b and c cleavage poles fall on girdles about SSW-plunging axes (F_6 folds) (also see Fig. 10). (b) Several generations found on a single, planar S_2 surface (dashed line); axes and poles to corresponding cleavages labeled with same letters. For each S_2 plane, age of cleavage decreases alphabetically. (c) Anti-clockwise-younging crenulation lineations (A—oldest, D–youngest). Scatter of poles to cleavages and lineations reflect formation on multiply folded surface (see text). (d) Same notation as for (b) but for crenulations related to dextral shear.

gently warped or folded (Figs. 8b & c). It should be noted that these cleavages usually are not axial planar to the clockwise-younging folds and that the time of formation of the first two cleavages (a and b) relative to the folds is not always the same across the island. The oldest cleavage (a) is approximately axial planar to F_5 folds in many cases (Figs. 5f and 8d) and is always folded by F_6 and F_7 folds. The next oldest cleavage (b) also pre-dates F_6 folds. In a few areas this cleavage (b) is nearly axial planar to F_5 folds (Fig. 7d), and the older cleavage (a) is reoriented around F_5 folds. The youngest cleavages of the clockwise-younging sets (c and d) are always post-F_6 and pre-F_7. These age relationships relative to the F_5–F_7 folds are reflected in the distributions of crenulation cleavage poles on the stereoplot in Fig. 11(a) and are illustrated on the map in Fig. 10 (large pull-outs labeled b, c & d).

Crenulation cleavage lineations (axes) on S_2 clearly show the consistent clockwise younging of the earliest cleavages (Figs. 10 and 11a). The map in Fig. 10 shows only enough lineation data to illustrate the important points; the general distribution and abundance of each crenulation generation has been maintained. At least three of these cleavages are present everywhere south of the SSC boundary; north of this boundary, three to four cleavages are localized in the discrete N- to NNE-trending shear zones. As the crenulation cleavages (and minor folds) are more abundant than the major F_5–F_7 folds north of this boundary (see Fig. 9), the distribution of the cleavages on Fig. 10 better illustrates the presence of the discrete shear zones. Unlike the folds, the orientation of the cleavage lineations does not indicate the orientation of the shear zone. These cleavages have been folded at least once, and most formed on folded surfaces. If the later folds are removed from any one S_2 surface cut by these crenulation cleavages, the unfolded orientations of the cleavages indicate shearing on N- to NNE-trending zones. Without unfolding each individual S_2 surface, the cleavages only show the sense of shear, not the orientation of the shear plane.

The consistent clockwise-younging relationship shown by the lineations also holds for the cleavages

themselves. On Fig. 10, the small pull-outs on the eastern side of the island show strikes and dips for three pairs of cleavages: (a–b, b–c, c–d), illustrating that the geometric relationships between cleavages and the correspondong lineations is the same. The younging of the cleavage generations is also shown on the stereoplot in Fig. 11(a). The trends of the cleavage lineations and strikes of the cleavages themselves young clockwise, similar to that shown by the mesoscopic folds. Cleavage planes also appear to become shallower as the cleavages become younger (clockwise younging) (Fig. 11a). This relationship is not just a reflection of the degree of folding. Figure 11(b) shows five planar S_2 surfaces that are crenulated by two or three cleavages. The lineations (marked on the S_2 surfaces with the age relationships indicated) clearly show clockwise younging of the axes. The poles to the cleavages corresponding to a single planar S_2 surface (labeled to match the axes) either show no change in dip or a systematic change with dips becoming shallower as the cleavages become younger. (The exception h, i has been completely overturned by folding.)

In summary, four clockwise-younging superposed cleavages are found on the island. The cleavages are pervasive south of the SSC boundary and are localized within discrete N- to NNE-trending zones north of this boundary. The cleavages have been folded by one or more of the F_5–F_7 folds, and thus their present orientation does not reflect the orientation of the shear zone. The superposed crenulation cleavages show the same sinistral sense of shear as the superposed mesoscopic folds and other kinematic indicators and provide an important kinematic indicator in these shear zones.

The discrete sinistral shear zones found on the northwest side of the island north of the SSC boundary contain mesoscopic folds in orientations oblique to all major fold trends (Fig. 2). These folds are found only in the coarse-grained lithologies within sinistral strike-slip shear zones that trend N18°E to N27°E. The folds generally trend S60°E with plunges from 30°SE to 85°SE and S30°E with plunges from 18°SE to 60°SE and are called F_3 and F_4, respectively (no chronologic order implied). F_3 and F_4 affect a pronounced foliation (Fig. 4c) and rarely have an associated axial planar crenulation cleavage. The folded foliation could be either S_1 or S_2; in the coarse-grained lithologies these foliations are difficult to distinguish. The folds are isolated within the shear zones; thus their orientation and relationship to folds outside the zone cannot be determined. The origin and deformational history of these folds remains unknown. The trend and steepness of the plunges for F_3 and F_4 folds vary with shear zone and with position within an individual zone. This variation suggests that these folds have been reoriented as a result of later shearing. The orientation is similar to that of F_2 folds outside of the zones in the northwestern part of the island. The trend of F_2 folds elsewhere on the island is generally SSE. Folds in this orientation could rotate into a SE orientation during sinistral shearing on these shear zones. F_5 or any later sinistral-related folds are not possibilities, as they formed at a clockwise angle to the shear plane and rotation during sinistral shear could not rotate these folds to a SE orientation. The pre-existing F_2 folds would be rotated toward the kinematic *a* direction; however, the steep plunges require both dip-slip and strike-slip movement on these shear zones. The combined rotations would cause reorientation into SE orientations and abnormally steep plunges. The direction of plunge for F_3 and F_4 indicates that the east side of NNE-trending shear zones moved down with respect to the west side. The rotation of F_2 folds by oblique-slip movement would produce folds at a high angle to the major structural trends. The orientations of these anomalous folds would be dependent on the amount of original deviation from horizontality of the axial planes or on the magnitude of the dip-slip component along the shear zone. The possibility that these folds are remnants of a discrete folding phase or phases that occurred between F_2 and F_5 cannot be ruled out. However, several other lines of evidence indicate dip-slip motion accompanied the sinistral strike-slip motion: (1) sinistral fold generations (F_5–F_7) show a progressive increase in plunge with age (see Fig. 9), suggesting a considerable dip-slip component was present on most shear zones; (2) field measurements of slickensides on fault planes indicate oblique-slip movement (Fig. 3). Athough no faults show demonstrable sinistral offset, seven oblique-slip faults in the northwest lie within and parallel sinistral shear zones; and (3) over a third (38%) of the kink bands found on the island are spatially related to N- to NNE-trending faults. These kink bands trend SSE to SSW and show a dip-slip motion (77% with the east side up). In many cases, these kink bands are folded by D_4 folds, and D_4 crenulation cleavages are only found on one limb of the kink band. D_3 sinistral crenulation cleavages are kinked by these bands. Thus, these kink bands are pre-D_4 structures and post-date some D_3 structures, confirming some dip-slip component of motion along approximately N-trending zones late in D_3.

The component of E–W extension indicated by the dip-slip motion is supported by one of two distinct generations of boudins that were mapped on Dutch Island. The first generation has N-trending neck lines and shows extension parallel to S_2. Examples of these structures are found throughout the field area, affecting both S_1 and S_2. The boudins were folded by both late stage D_3 and all D_4 deformation. Removal of this subsequent deformation indicates an E–W extension direction. The timing and orientation of these boudins suggests that the first phase of boudinage was associated with sinistral shearing, and occurred early during D_3.

In summary, sinistral, oblique-slip movement on NNE-trending zones is indicated by multiple generations of superposed mesoscopic folds and crenulation cleavages that show a consistent clockwise younging and other more conventional indicators. This sinistral deformation increases in intensity southward. North of the SSC boundary, discrete sinistral shear zones are found, whereas south of this boundary, the sinistral-related structures are pervasive but increase in number and

intensity approaching some NE-trending shear zones. These NE-trending zones and adjacent structures appear to have been rotated into this orientation from a N to NNE-trend. On the northwestern side of the island, the dominant major structures are steeply SE- to SSE-plunging F_3 and F_4 folds that most likely represent highly reoriented F_2 folds. Southwards, major S- to SSW-plunging F_5–F_7 folds become more abundant, and F_1 and F_2 folds are completely transposed.

DEXTRAL SHEAR INDICATORS

Dextral movement (D_4) on NE- and ENE-trending shear zones and faults followed the sinistral strike- and oblique-slip movement (D_3). Vertical strike- and oblique-slip shear zones and faults trending NE to ENE with measurable offset or kinematic indicators showing dextral motion were mapped on Dutch Island (Figs. 2 and 3). Kinematic indicators include sheath folds, en échelon folds, tension gashes, superposed anti-clockwise-younging mesoscopic folds and crenulation cleavages, and small-scale subsidiary shear zones within major zones that show measurable ductile offset. Additionally, D_3 structures swing into the dextral shear zones indicating clockwise rotation. This overprinting of sinistral-related structures by dextral deformation is best shown on Fig. 9. As F_5–F_7 folds approach major dextral zones, the orientations gradually change reflecting clockwise rotation toward the shear plane. Some individual fold axes can be traced into dextral zones, and the axes are clearly bent by the dextral motion. The effects of dextral movement increase southward on the island. For example, just south of the SSC boundary on the western side of the island, major structures are S- to SSW-plunging F_5–F_7 folds. These structures gradually swing into SW orientations approaching a major dextral shear zone (labeled 3 on Fig. 9). In the center of this shear zone, folds are nearly parallel with the trace of the shear zone. Similar reorientation of the sinistral-related crenulation cleavages can be seen on Fig. 10. Brittle faults are located in the center of major dextral zones at the southern end of the island (compare Figs. 3 and 9). These faults show oblique-slip dextral motion with the south side up. Shear zones adjacent to NE-trending faults (e.g. Figs. 5c & d) are wider than those adjacent to ENE-trending faults (e.g. Figs. 4h and 5b), and both show the same sense of shear as the measurable offset.

Within dextral shear zones are a set of mesoscopic superposed folds (F_8–F_{11}) of approximately 2–5 cm amplitude. All of these folds may be characterized as open, doubly plunging folds (Figs. 5e and 7a) that visibly affect all of the previously existing structures. The folds exhibit clear cross-cutting relationships and consistent internal geometries. Folds young in an anti-clockwise direction (Fig. 12), and younger folds are slightly more open than older folds. These folds are only found on E-dipping surfaces and are best expressed where dips are shallow to moderate (Figs. 5c & e). Where S_2 changes from vertical to moderately E-dipping, as a result of F_6 folding, the F_8–F_{11} folds are found only on moderately dipping limbs (Fig. 5c). This relationship shows that F_8–F_{11} folds post-date F_6 folds.

Cross-cutting relationships for F_8–F_{11} are not as easy to demonstrate as those for sinistral-related folds because F_8–F_{11} are similar in size and occur on a smaller scale than the F_5–F_7 folds. Thus, the axial planes of early folds do not vary across an outcrop in response to later folding. Instead, F_8–F_{11} folds are usually seen on a single S_2 surface, and the depth of their penetration in cross-section is unknown. Rare joint surfaces cut these folds allowing axial planes to be measured and the penetrative nature (in cross-section) of folds to be seen (Figs. 5c & e). Overprinting relationships between these folds are subtle as is illustrated in Figs. 7(a)–(c). F_8 folds appear to die out after changing trend (Fig. 7a, above hammer

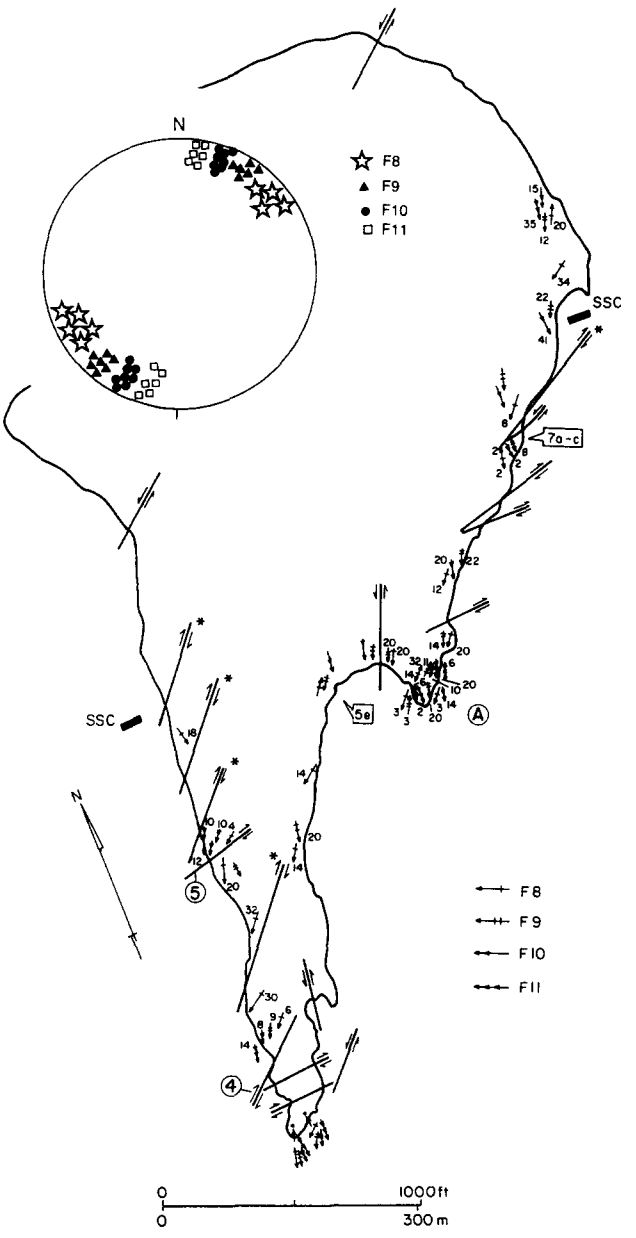

Fig. 12. Structural map of minor F_8, F_9, F_{10} and F_{11}. Folds found only within dextral shear zones; folds away from major zones are within minor discrete dextral zones. Stereoplot shows fold axes rotated to horizontal surface; axial planes rarely exposed. (For shear zones 4 and 5, see Table 1; area A discussed in text.) Locations of Figs. 5(e) and 7(a)–(c) shown.

handle) where cross-cut by oblique F_9 folds. The trend change occurs crossing the F_9 antiforms and the folds appear to die out crossing the F_9 synforms (Fig. 7c). Similar types of interference relationships also are observed where F_{10} cross-cut F_9 and F_8 folds. The difference in amplitude of the older folds on opposite limbs of the younger folds is well shown in Figs. 7(a)–(c) (near B in Fig. 7a) where only a faint indication of the F_8 folds can be seen on the lower limb of an F_{10} fold. This overprinting causes the doubly plunging character of these fold generations. In some places the axial planes of the younger folds can be seen to be folded. For example, an F_8 axial plane in Fig. 7(c) is folded by F_9 (trace F_8 fold at pen tip up to south), confirming the sequence of folding. Because the folds are open and of the same scale, the axial planes of early ones are only gently warped (Fig. 5c) by the later ones at the intersections of the two fold generations. Away from the intersection, the earlier fold axial planes are not folded (Fig. 5e). The relationship between these later folds are similar in outcrop and hand sample to those shown in Figs. 5(f)–(h) for small-scale F_5 and F_6 folds.

Although the geometric relationships among these fold generations are distinctive, they are morphologically very similar (Figs. 5e and 7a & c). The overall geometric similarity between all of the folds, which appear almost 'ripple-like' or anastomosing in nature, might make this deformation a likely candidate for progressive deformation caused by inhomogeneous strain or lithologic variation (Ramberg 1964). However, the consistent overprinting relationships that these folds display, their presence only in shear zones, and the overall lithologic homogeneity of the Dutch Island phyllites seem to preclude this possibility. Instead, folds F_8–F_{11} represent folds produced by progressive increments of deformation and subsequent rotation within a dextral shear couple. Thus, dextral fold generations formed sequentially at an angle to the shear plane, as did the sinistral folds, and were rotated internally in a clockwise direction (Fig. 6b).

The consistent anti-clockwise younging of F_8–F_{11} is shown on the map and stereoplot in Fig. 12. In contrast to the F_5–F_7 folds on Fig. 9, these are small-scale folds. Because these folds are morphologically similar, when only one is present, it is called F_8; when two are present they are called F_8 and F_9, and so on. Note that these folds are not as abundant as F_5–F_7 folds, and they are nearly non-existent on the northwest side of the island. The presence of one particularly complex area (A on Fig. 12) strongly suggests that a major dextral shear zone lies just offshore and that the minor zones observed in this area are small, subsidiary zones.

Dextral fold and rotation data for two shear zones are summarized in Table 1 and indicate a swing in fold axis orientations between NE- and ENE-trending shear zones. Adjacent to NE-trending zones, the angular relationship between the folds and the shear planes are similar to those described for sinistral shearing. Along ENE-trending zones, however, the angles between respective dextral folds and the shear planes are markedly higher. Two possibilities could account for this difference: (1) less shearing has occurred along ENE-trending shear zones than along NE-trending zones, hence angles between the folds formed as a result of shear and the shear plane are greater; (2) the shearing along NE-trending shear zones formed the folds before ENE shearing began, and those folds were later rotated during ENE shearing. The first possibility is supported by the narrower width of ENE-trending zones. However, the second possibility is most likely because the angle between F_{11} and the shear plane for the ENE-trending zones is greater than 45°, making a genetic relationship between these structures unlikely. In addition, there is no direct interference pattern among dextral fold generations at junctures between NE- and ENE-trending shear zones; rather, a gradual swing in fold axis orientation toward the ENE shear plane is observed, suggesting later reorientation.

Geometric analysis of Dutch Island crenulation cleavages and lineations on the S_2 surface indicates that NE- to ENE-trending shear zones show a dextral shear sense, similar to other kinematic indicators. The crenulation cleavages young in an anti-clockwise direction; this relationship is well illustrated in Fig. 7(b) where N-plunging crenulation lineations are folded by S-plunging ones. In thin section, overprinting relationships among anti-clockwise younging generations and among anti-clockwise and clockwise-younging generations can be determined. Either a young cleavage folds an older one (old one can be traced through the fold; Figs. 8f & h) or a young cleavage is present on only one limb of an older crenulation because the other limb is in an orientation inappropriate for microfolding (Figs. 8d, e & g). For example, in Fig. 8(g), crenulation C is only expressed on the limb of crenulation B where S_2 is at a high angle to C and not on the limb where S_2 is nearly parallel to C. These relationships are observed on all scales (Figs. 7d & e).

The consistent anti-clockwise-younging of the crenulation lineations on S_2 is shown on the map in Fig. 10. These cleavages are found only within dextral shear zones and are not as abundant as the clockwise-younging cleavages associated with sinistral shear zones. At the southern tip, four anti-clockwise-younging cleavage generations can be found, however, elsewhere no more than three are found together (Fig. 10). Cleavages strike from NNE to NE and show the same anti-clockwise-younging relationship as the lineations (see small pull-out of northeast coastline on Fig. 10). The lineations plunge SSE to SSW, because S_2 generally strikes NNE and dips east.

Orientations of crenulation lineations (axes) vary greatly with the orientation of the surface on which they are found (Figs. 10 and 11c). Although different generations overlap more in lineation orientation than the clockwise-younging lineations (compare Figs. 11a & c), at a single location or on a single planar S_2 surface, the younging is consistent (Figs. 10 and 11d). No consistent relationship between the anti-clockwise-younging folds and cleavages was found. For example in Fig. 7(c), most

lineations (except for one subparallel to F_{10}) are not coaxial with the folds and are folded. Folds of the cleavages, when present, are small scale and do not affect the orientations of the cleavages appreciably. Although this folding may cause some of the scatter in orientation of the cleavages observed on the stereoplot in Fig. 11(c), the orientation of the surfaces on which they form have more effect. These crenulation cleavages form on S_2 surfaces previously folded by large F_5–F_7 folds. The oldest and steepest (75–85°E) dipping cleavages generally form on horizontal limbs, the intermediate in age and dip (60–65°E) form on limbs with moderate dips, and the youngest and shallowest (30–47°E) form on limbs with steeper dips; none form on very steep to vertical dips (see for example, Fig. 7d). This relationship presumably occurs because it is easiest to form the crenulation cleavages on horizontal planes, and vertical planes are in the wrong orientation to be crenulated (as they are for F_8–F_{11} folding). Thus, as deformation progresses, cleavages form on surfaces that are increasingly less appropriately oriented for (micro-) folding. In general, cross-cutting cleavages formed on the same S_2 plane have the same dips, but in some cases, dips became shallower (in an anti-clockwise manner) as the cleavages become younger (Fig. 11d). In these cases, a dip-slip component to the shearing is indicated. (Note these cleavages have not been folded, unlike those related to sinistral shearing.)

Crenulation cleavages were especially useful in identifying zones that show both sinistral and dextral motion. Some NE-trending zones south of the SSC boundary show sinistral motion preceding dextral motion. In these cases, dextral crenulation cleavage sets are found only within the shear zones, whereas sinistral crenulation cleavages also are found between NE-trending zones (Fig. 10; e.g. zones in area labeled A), although they intensify as these zones are approached. Within the zones, dextral crenulation cleavage sets overprint the sinistral sets. The technique used to determine the sequence of events within zones with more than one sense of motion involved tracing a given sinistral set of crenulation cleavages into a zone (map scale of 1:60) and determining the overprinting relationships relative to the dextral generations.

The major NE-trending dextral shear zones show no significant dip-slip component, although some dextral faults in this orientation show oblique-slip offset (Fig. 3). In contrast, the ENE-trending shear zones usually show a dip-slip component, best expressed by localized reorientation of adjacent structures (Fig. 4h), and faults in this orientation show oblique-slip offset and slickensides (Figs. 3 and 5c & d). Dip-slip motion is also indicated by E-trending tension gashes (Figs. 7a & c) and E- to ESE-trending kink bands spatially associated with these faults (41% of the kink bands on the island; 79% show north side up)

Some blocks bounded on two sides by ENE-trending dextral, oblique-slip faults apparently underwent rigid-body rotation on steeply plunging axes. Such rotation could be identified because of the degree of consistency of internal geometries for superposed, mesoscopic folds and crenulation cleavages. Discrimination of subtle changes in orientation of fold and cleavage sets across faults indicated between 8 and 10° of rigid-body rotation on steeply plunging axes. For example, the F_5–F_7 folds measured in one fault-bounded outcrop (labeled A on Fig. 9) are rotated anti-clockwise relative to those on either side of the faults, and the crenulation cleavages between two faults on the southern tip of the island show an abrupt change in orientation across the faults indicating a clockwise rotation (pull-out of lineations in Fig. 10). Abrupt changes in orientations of structures across the fault labeled 2 on Fig. 9 suggests some rigid rotation occurred along this fault. In each case, the changes in orientation of the structures indicates that outcrops were externally rotated (or rotated as discrete blocks) by fault motion after ductile deformation producing the fold and crenulation sets had occurred.

Following the dextral shearing, a second phase of boudinage showing N–S extension occurred. All outcrops have been warped during boudinage on steeply plunging axes ranging in trend from ESE to E to N60°E. The distance between boudin necks is up to 10 m in cross-sectional view. In a few cases, the ESE- and N60°E-trending boudin necks form en échelon arrays, with each neck extending only for a few feet along its length (e.g. Fig. 7a). Some of the boudins show evidence of two increments of extension in which opening occurred along E-striking planes, the first dipping south at about 45° opening north over south and the second dipping north at about 45° opening south over north, indicating at least a local change in strain orientation during boudinage. These boudins erode to a curious 'dimple-like' pattern along prominent sea cliffs allowing superposition relative to other structures to be determined (Fig. 7a). The boudins visibly affect folds related to both sinistral and dextral shear, as well as all prominent crenulation cleavages. In some broad necks of boudins, conjugate sets of kink bands (21% of those on the island; Figs. 7a & c) are found. Although the boudinage post-dates the dextral-related structures, the extension direction for this second generation of boudins is appropriate for dextral shear, suggesting that the boudinage was a late phase of the D_4 deformation.

In summary, deformation related to dextral shearing increases in intensity to the south and reorients the earlier sinistral structures. Dextral movement on NE-trending zones is indicated by multiple generations of superposed mesoscopic folds and crenulation cleavages that show a consistent anti-clockwise-younging and other more conventional indicators. These structures are reoriented by subsequent dextral oblique-slip movement on narrower, ENE-trending zones (and faults). North–south extension causing widespread boudinage followed the NE-trending dextral deformation and may be associated with the late-stage dextral deformation. Some discrete blocks bounded by faults show evidence of late-stage rigid-body rotation.

DISCUSSION

Tectonic interpretation

The complex structure found on Dutch Island was formed as a result of strike- and oblique-slip movement along a system of non-parallel shear zones, overprinting a well-developed metamorphic and structural fabric. Considerable amounts of whole block rotation measured in discrete blocks around the island suggest that the island as a whole may have acted as a large block caught up and rotated in a complex shear zone system. Clearly, a question remains as to the regional significance of a locally complicated structural problem. The shear zone trends and movement directions must be present away from the island to extrapolate strain history information to the Narragansett Basin at large. If the major shear zone trends observed on Dutch Island are not unique within the basin, then a detailed structural analysis of the island would help to determine the large-scale strains that were acting on the basin during late-stage deformation.

The shear zone trends and motions measured on Dutch Island may be summarized (in chronological order) as follows: sinistral strike- and oblique-slip motion on NNE-trends, dextral strike-slip motion on NE-trends, and dextral oblique-slip on ENE-trends. For NE-trending zones that underwent both sinistral and dextral motion, sinistral movement always preceded dextral movement. These zones apparently represent NNE-trending sinistral zones that were rotated into a NE-trend by subsequent dextral shearing. (Sinistral motion is termed D_3 and dextral D_4.) The most pervasive ductile deformation is that related to sinistral movement on NNE-trending shear zones. However, dextral motion on NE-trending zones was significant, causing ductile reorientation of all earlier structures and formation of new minor (ductile) structures. The oblique-slip dextral motion on ENE-trending zones caused the least ductile deformation and the most brittle offset. The latter may be associated with N–S extension that produced the late-stage boudinage. Thus, with time, deformation became less ductile and the active shear plane orientation rotated clockwise.

D_3 and D_4 deformation is locally observed elsewhere in the basin within similar trending shear zones and adjacent to faults (Burks 1981, 1985, Henderson & Mosher 1983, Mosher 1983, unpublished work). Although not all shear zones contain faults, the increase in intensity of D_3 and D_4 deformation approaching faults suggests that ductile shearing of a large area occurred prior to fault formation. The orientations of the shear zones and faults on Dutch Island and elsewhere in the basin are parallel to high-angle basement faults that bound intrabasinal horsts and grabens (Mosher 1983, Henderson & Mosher 1983). This correspondence suggests that the D_3 and D_4 deformation results from strike-slip reactivation of pre-existing, high-angle basement faults bounding intrabasinal horsts and grabens.

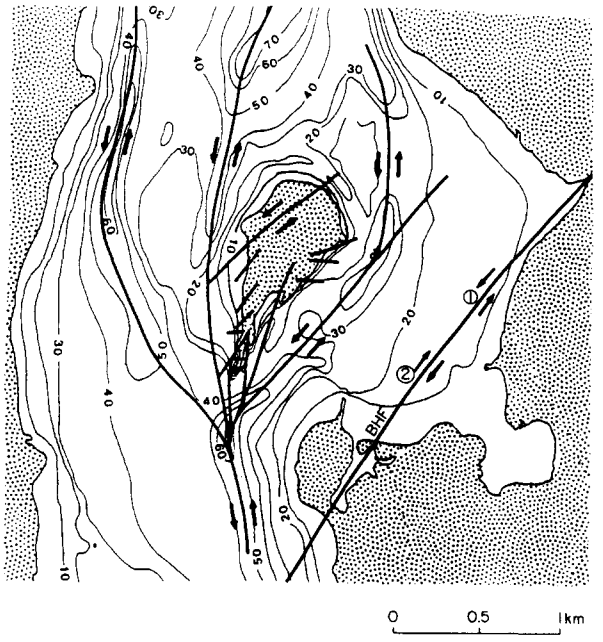

Fig. 13. Composite map of basin bathymetry (after Henderson unpublished work) showing depth to basin floor in feet and known and inferred faults or shear zones on and around Dutch Island. (Land dotted pattern.) Note prominent linear lows around Dutch Island, corresponding to major strike-slip fault localities, and complex splay system south of island, producing both sinistral and dextral faults and shear zones.

As these faults are reactivated, the overlying metasediments would first be sheared in a ductile manner. With increasing displacement, the metasediments directly overlying the faults would undergo the most strain. When coupled with strain hardening, an increase in strain rate, decreasing temperatures, or even larger displacements, faults with the same sense of motion would cut through the ductile shear zones. This sequence best fits the widespread ductile D_3 and D_4 structures observed on Dutch Island and elsewhere in the basin.

A map of basin bathymetry around Dutch Island constructed by M. C. Henderson (Fig. 13), shows trends of topographic highs and lows on the basin floor around the island. These trends form lineaments in the same general orientations as fault and shear zone orientations mapped on Dutch Island, and often appear to be offshore extensions of structures measured on the island. Under water examination of some of these lineaments around Dutch Island confirmed that they were indeed faults. This information, combined with gravity and magnetic data collected for the southern Narragansett Basin, strongly indicate that the fault and shear zone trends observed on Dutch Island are present immediately adjacent to the island, as well as in outcrop elsewhere in the basin (Skehan & Murray 1979, Burks 1981, Henderson & Mosher 1983, Mosher 1983). A composite map of shear zones on Dutch Island and submarine faults inferred from basin topography and geophysical data (Fig. 13), and confirmed in places while scuba diving, presents an overview of faulting on and around the island. A major N- to NNE-trending fault (and

possible shear zone) bends and splays immediately south of Dutch Island. Shear zones in this orientation on the island are sinistral, hence these faults are considered sinistral. The subsidiary faults formed at the splay could account for the extreme structural complexity in the southern part of the island. Other major lineaments surrounding the island are similar in orientation to mapped faults and shear zones on land, suggesting possible offshore counterparts, if not extensions, of these faults. The fault pattern observed on Dutch Island could allow for some whole block rotation in the southern part of the island, although similarities in fold and fault orientations around the island would preclude any significant rotation on greater than outcrop scale.

The large amount of strike-slip deformation on Dutch Island and elsewhere in the Narragansett Basin late in the Alleghanian orogeny after collision of Africa with North America suggests that the shear zone patterns on the island may be part of sinistral or dextral transform systems, active in the Late Paleozoic. Relative motions and orientations of the faults underlying the shear zones on Dutch Island could be analogous to R' Riedel and primary (P) shears within a larger E-trending dextral shear zone, as proposed by Mosher (1983) and Berryhill (1984). In this model, initial NNE-trending, sinistral zones would be R' Riedel shears, and ENE-trending, dextral zones would be primary shears. Zones corresponding to R Riedel shears were not documented. Zones presently trending NE are explained as pre-existing basement faults that were originally oriented more northerly and were reactivated first as R' Riedel shears. With continued shearing these faults, which were oriented more easterly than was appropriate for R' Riedel shearing, rotated into a NE-trend where dextral motion predominated.

Several problems with this model include: (1) most experiments show P shears form at large strains in areas containing R shears and not in areas with R' shears (see Freund 1974); (2) the explanation of NE-trending, sinistral then dextral zones is plausible but not completely satisfactory; (3) more dextral movement occurred on NE-trending zones than ENE-trending zones; and (4) the ENE-trending dextral zones are dominantly dip-slip and show similar extension directions as the late-stage boudinage. The latter two facts are more compatible with a NE-trending transform system. Thus, a more likely model is that a sinistral, NNE-trending transcurrent shear zone system was active first and was subsequently cut by a dextral NE-trending transcurrent shear zone system. In this model, the early sinistral shearing (D_3) reactivated pre-existing basement faults with a northerly trend causing ductile deformation of the overlying metasediments, and later dextral shearing (D_4) reactivated NE-trending faults, locally rotating the overlying, SSW-plunging folds and shear zones into a SW trend. Then with increasing strain, pre-existing E-trending faults underwent extension forming boudins and dip-slip faults with a slight dextral component in the overlying metasediments. Late-stage Alleghanian dextral motion also has been documented for the adjacent basement (e.g. O'Hara & Gromet 1985, Getty & Gromet 1988, Wintsch & Sutter 1986, Goldstein 1989) and is compatible with that observed in the Narragansett Basin (for discussion see Reck & Mosher 1989). The earlier sinistral motion, however, has not been recognized in the basement. A switch from sinistral to dextral motion on transcurrent shear zones (and faults) along the boundary between two large continents (Africa and North America) soon after collision is not surprising, and further work on late-stage Alleghanian deformation should delineate the extent of early sinistral transcurrent motion and will help in our understanding of the complex interactions at colliding plate boundaries.

Kinematic indicators

Structural analysis of the complex shear system on Dutch Island shows that accurate tracking of the movement history is possible if overprinting relationships between progressively formed structures are preserved. In response to strike-slip motion along nearly vertical shear zones, the pre-existing, nearly horizontal S_2 foliation was folded (or crenulated). Folds apparently initiated at angles slightly greater than 30° to the shear plane and rotated towards the kinematic a direction. At least 26° of internal rotation of mesoscopic folds and crenulation cleavages occurred within sinistral and dextral shear zones. Fold rotation toward the shear plane continued until the fold could no longer accommodate the strain because of its orientation relative to the incremental strain axes. A new fold generation then formed at slightly more than 30° to the shear plane and overprinted the earlier (and presently locked) generations. Between 6 and 18° of internal rotation can occur prior to initiation of a new generation of folds (or crenulations). In addition, as much as 10° of external, whole block rotation affected structures on parts of the island after the ductile shearing. This study has shown that non-coaxial, non-coplanar, consistently younging folds and crenulation cleavages can provide accurate kinematic indicators in shear zones, and unlike many indicators, clear superposition of opposite senses of motion and the relative timing of the different motions can be determined.

CONCLUSIONS

The deformation on Dutch Island produced the most intense and complex set of structures observed in the Narragansett Basin. Four major deformational events are preserved in the metasediments, corresponding to the four major deformations recorded elsewhere in the basin. Late-stage deformation is localized along a system of non-parallel, intersecting strike- and oblique-slip shear zones with opposite senses of motion. Sinistral shear zones occur in NNE to NE orientations, and dextral shear zones in NE to ENE orientations. Structural superposition of mesoscopic folds and incremental crenulation cleavages, formed as a result of progressive

movement along these zones, indicates that sinistral motion preceded dextral motion and that many shear zones which presently trend NE underwent first sinistral then dextral movement. The latter zones apparently were NNE-trending sinistral zones that were reoriented into a NE-trend during later dextral shearing. The dextral motion on NE-trending zones preceded similar motion on ENE-trending zones with the latter showing considerable dip-slip motion. Faulting post-dated ductile shearing and showed the same directions of motion suggesting the faults were part of the progressive deformation. Rigid whole-block rotation on ENE-trending faults also post-dated the ductile deformation. Deformation became increasingly brittle with time: the most pervasive and large-scale ductile structures are related to the early NNE-trending shear zones; only minor new ductile structures are associated with the NE-trending zones, but these zones show large-scale ductile reorientations of previous structures; and narrow zones of ductile reorientation and brittle faults constitute the latest ENE-trending zones.

Structural analysis of the superposed mesoscopic folds and crenulation cleavages on Dutch Island indicates that accurate tracking of shear zone motion within complex shear systems is feasible in areas in which overprinting relationships between progressive deformations are preserved. As many as eight generations of discrete superposed crenulation cleavages and seven generations of discrete mesoscopic folds were developed on the island as a result of sinistral and dextral motion. Folds related to sinistral and dextral strike-slip motion on shear zones on Dutch Island formed at angles slightly greater than 30° to the shear plane, and the earliest folds were subsequently rotated approximately parallel to the shear plane. Study of geometry and overprinting relationships of the fold and crenulation generations within shear zones served to track movement along individual zones through time and allowed multiple motions and the timing of those motions to be distinguished. This complex sequence of structures was preserved as a result of the formation of a strong structural and metamorphic fabric early in the deformational history of the island.

The deformation recorded on Dutch Island can best be explained by early NNE-trending sinistral and later NE-trending dextral transcurrent shear zone systems that are not related to a single transform fault system and demonstrates the complex plate interactions that occur after collision along the boundary between large plates. The structural styles and deformation patterns described on Dutch Island should be analogous to what might be expected in a larger block caught within a system of non-parallel transcurrent shear zones. This study also has documented that incrementally-formed, superposed crenulation cleavages provide a powerful, new kinematic indicator for pelitic rocks.

Acknowledgements—We would like to thank Drs Rachel J. Burks, William R. Muehlberger, William Carlson and Mark Cloos for many helpful discussions during the initial research. The paper benefited from helpful reviews by Drs Donald Secor and James Skehan and an anonymous reviewer. Funding for the field portion of this study was provided through a National Science Foundation Grant (EAR-811-1294). Lodging while in the field was provided by Ft. Getty Recreation Area and the town of Jamestown, Rhode Island. Special thanks go to Jeff Horowitz for the drafting, David Stephens for the photography, and Betty Kurtz for the typing.

REFERENCES

Berryhill, A. W. 1984. Structural analysis of progressive deformation within a complex strike-slip fault system: southern Narragansett Basin, Rhode Island. Unpublished M.A. thesis, University of Texas at Austin.

Burks, R. J. 1981. Alleghenian deformation and metamorphism in Narragansett Basin, Rhode Island. Unpublished Master's thesis, University of Texas at Austin.

Burks, R. J. 1985. Incremental and finite strains within ductile shear zones, Narragansett Basin, Rhode Island. Unpublished Ph.D. dissertation, University of Texas at Austin.

Farrens, C. M. 1982. Styles of deformation in the southeastern Narragansett Basin, Rhode Island and Massachusetts. Unpublished Master's thesis, University of Texas at Austin.

Freund, R. 1974. Kinematics of transform and transcurrent faults. *Tectonophysics* **21**, 93–134.

Getty, S. R. & Gromet, L. P. 1988. Alleghanian polyphase deformation of the Hope Valley Shear Zone, Southeastern New England. *Tectonics* **7**, 1325–1328.

Goldstein, A. G. 1989. Tectonic significance of multiple motions on terrane-bounding faults in the northern Appalachians. *Bull. geol. Soc. Am.* **101**, 927–938.

Grew, E. S. & Day, H. W. 1972. Staurolite, kyanite, and andalusite from the Narragansett Basin of Rhode Island. *Prof. Pap. U.S. geol. Surv.* **800-D**, 151–167.

Henderson, M. C. & Mosher, S. 1983. Narragansett Basin, Rhode Island: role of pre-existing intrabasinal horsts and grabens in Alleghanian deformation (abstract). *Geol. Soc. Am. Abs. w. Prog.* **15**, 129.

Mahler, J. P. 1988. Late-stage Alleghanian wrenching of the western Narragansett Basin, Rhode Island. Unpublished Master's thesis, University of Texas at Austin.

McMaster, R. L., de Boer, J. & Collins, B. P. 1980. Tectonic development of southern Narragansett Bay and offshore Rhode Island. *Geology* **8**, 496–500.

Mosher, S. 1976. Pressure solution as a deformation mechanism in Pennsylvanian conglomerates from Rhode Island. *J. Geol.* **84**, 355–364.

Mosher, S. 1983. Kinematic history of the Narragansett Basin, Massachusetts and Rhode Island: constraints on late Paleozoic plate reconstructions. *Tectonics* **2**, 327–344.

Mosher, S. 1985. Effects of Alleghanian accretion to the Boston platform on the western Narragansett Basin, Rhode Island (abstract). *Geol. Soc. Am. Abs. w. Prog.* **17**, 670.

Murray, D. P. & Mosher, S. 1984. Permian deformation and metamorphism in southwestern New England (abstract). *Geol. Soc. Am. Abs. w. Prog.* **16**, 53.

Mutch, T. A. 1968. Pennsylvanian non-marine sediments of the Narragansett Basin of Massachusetts and Rhode Island. In: *Late Paleozoic and Mesozoic Continental Sedimentation, Northeastern North America* (edited by deVries, Klein, G.). *Spec. Pap. geol. Soc. Am.* **106**, 177–209.

O'Hara, K. & Gromet, L. P. 1985. Two distinct late Precambrian (Avalonian) terranes in southeastern New England and their late Paleozoic juxtaposition. *Am. J. Sci.* **285**, 673–709.

Ramberg, H. 1964. Selective buckling of composite layers with contrasted rheological properties, a theory for simultaneous formation of several orders of fold. *Tectonophysics* **1**, 307–341.

Ramsay, J. G. 1980. Shear zone geometry: a review. *J. Struct. Geol.* **2**, 83–99.

Reck, B. H. 1985. Deformation and metamorphism in the southwestern Narragansett Basin and their relationship to granite intrusion. Unpublished Master's thesis, University of Texas at Austin.

Reck, B. H. & Mosher, S. 1989. Timing of intrusion of the Narragansett Pier Granite relative to deformation in the southwestern Narragansett Basin, Rhode Island. *J. Geol.* **96**, 677–692.

Shaler, N. S., Woodsworth, J. B. & Foerste, A. F. 1899. Geology of the Narragansett Basin. *U.S. geol. Surv. Monogr.* **33**.

Skehan, S. J. & Murray, D. P. 1979. Geology of the Narragansett Basin, southeastern Massachusetts and Rhode Island. In: *Carbon-*

iferous Basins of Southeastern New England (edited by Cameron, B.). American Geological Institute, Falls Church, Virginia, 7–35.

Skjernaa, L. 1980. Rotation and deformation of randomly oriented planar and linear structures in progressive simple shear. *J. Struct. Geol.* **2**, 101–109.

Thomas, K. J. 1981. Deformation and metamorphism in the central Narragansett Basin of Rhode Island. Unpublished Master's thesis, University of Texas at Austin.

Wintsch, R. P. & Sutter, J. G. 1986. A tectonic model for the late Paleozoic of southeastern New England. *J. Geol.* **94**, 522–539.